




**Thin film extensional flow of a transversely isotropic viscous fluid**M. J. Hopwood,<sup>1,2</sup> B. Harding ,<sup>1,3</sup> J. E. F. Green ,<sup>1</sup> and R. J. Dyson <sup>2</sup><sup>1</sup>*School of Mathematical Sciences, University of Adelaide, Adelaide, South Australia 5005, Australia*<sup>2</sup>*School of Mathematics, University of Birmingham, Edgbaston, Birmingham B15 2TT, United Kingdom*<sup>3</sup>*School of Mathematics and Statistics, Victoria University of Wellington, PO Box 600, Wellington 6140, New Zealand*

(Received 15 November 2022; accepted 10 October 2023; published 3 November 2023)

Many biological materials such as cervical mucus and collagen gel possess a fibrous microstructure. This microstructure affects the emergent mechanical properties of the material and hence the functional behavior of the system. We consider the canonical problem of stretching a thin sheet of transversely isotropic viscous fluid as a simplified version of the spinnbarkeit test for cervical mucus. We propose a solution to the model constructed by Green and Friedman by manipulating the model to a form amenable to arbitrary Lagrangian-Eulerian (ALE) techniques. The system of equations, reduced by exploiting the slender nature of the sheet, is solved numerically, and we discover that the bulk properties of the sheet are controlled by an effective viscosity dependent on the evolving angle of the fibers. In addition, we confirm a previous conjecture by demonstrating that the center line of the sheet need not be flat, and perform a short timescale analysis to capture the full behavior of the center line.

DOI: [10.1103/PhysRevFluids.8.113301](https://doi.org/10.1103/PhysRevFluids.8.113301)**I. INTRODUCTION**

Fluids can be classified as isotropic, or anisotropic, depending upon whether the mechanical properties of the fluid are uniform in all directions or not. Most common fluids such as water are isotropic. However, there are many examples of fluids that arise in biology and industry which contain fibers or elongated particles, for example, collagen gels [1], cervical mucus [2], and nematic liquid crystals [3]. The presence of fibers or particles within the fluid creates an underlying structure that causes the fluid to exhibit anisotropy. The anisotropy of biological fluids means that they can display interesting behaviors and possess unusual and evolving mechanical properties, which influence how they perform their particular functions. For example, the anisotropy of cervical mucus is suspected to play a role in fertility by controlling how easily sperm can migrate through to the egg [4].

One of the first models of an anisotropic viscous fluid was formulated by Ericksen [5]. He considered a type of anisotropy known as “transverse isotropy” where the material possesses a single preferred direction which may vary both spatially and temporally; its physical properties are symmetric in all directions normal to this preferred direction. While, in general, for a fibrous material, one would need to consider the evolution (in time and space) of a probability distribution describing the alignment of a fiber along a particular direction, the Ericksen model simplified the problem by assuming that there is a unique fiber alignment at each point in space. Examples of materials that have been modeled using this approach include fiber-reinforced composites [6], entanglements of textile fibers used in the carding process [7], and a number of biological materials: collagen gels [1], the extracellular matrix [8], and primary plant cell walls [9]. A significant number of studies motivated by problems in composites manufacturing include the additional assumption that the fluid is inextensible in the fiber direction [6,10,11]; these are termed “ideal” incompressible fiber-reinforced fluids.

In this paper we consider the extensional flow of a thin sheet of transversely isotropic viscous fluid. One motivation for studying this problem is that it provides a simplified representation of the “spinnbarkeit” or “spinnability” test, which is applied to cervical mucus as a means of assessing fertility [12]. The test entails taking a sample of mucus and stretching it. Around ovulation, the mucus has a lower pH and a higher concentration of water (which has the effect of lowering the viscosity of the mucus), and the fibrous reinforcement takes a more parallel alignment that allows sperm to migrate. At this point the mucus can be stretched the furthest, i.e., the fluid exhibits maximum spinnbarkeit. Conversely, during the most infertile parts of the menstrual cycle, the mucus does not stretch and simply breaks [13,14]. Understanding the dynamics of stretching a transversely isotropic sheet can provide some basic insights into how factors such as fiber concentration and alignment influence spinnbarkeit. A second motivation for studying this problem is that it provides a simple prototype situation for investigating how the feedback between the macroscopic fluid flow and the microstructure influences the mechanical behavior of anisotropic fluids. In particular, as shown in [1], the model can be reduced to one dimension, with the changing orientation of the fibers specified by a single angle.

Extensional thin film flows of incompressible Newtonian fluids, which arise in a number of industrial and biological applications, have been extensively studied. The problem of a two-dimensional (2D) thin film was considered by Howell [15], who employed an asymptotic expansion of the Navier-Stokes and mass conservation equations in powers of an inverse aspect ratio to obtain a reduced model (termed the Trouton model) which involves only the leading order longitudinal fluid velocity and sheet thickness. Additionally, the roles of inertia and surface tension have been considered, as well as the complementary problems of fluid threads (i.e., slender cylinder) or drops [15–17]. In order to capture the full behaviors of the center line of the fluid of the sheet, a short timescale analysis is carried out [15,18,19]. These models are not valid for sheets undergoing deformation by bending and led to the development of a general theory for thin viscous sheets that undergo deformation by stretching, bending, or an arbitrary combination of both by Ribe [20,21]. This work was able to explicitly quantify relations between bending and stretching of the sheet. A complementary study considered sheets with an inhomogeneous viscosity [22]. One of their main results was that “necking” of the sheet, where regions of the sheet thinned faster than others, could be induced by in-plane variations of viscosity throughout the fluid. However, for a transversely isotropic fluid, we are aware of only three studies of extensional flow: those of [9,23], wherein both works modeled the primary plant cell wall as a thin axisymmetric fiber-reinforced viscous sheet supported between rigid end plates, and that of [1], who used a similar approach to that of Howell [19] to derive a transversely isotropic version of the Trouton model. The model presented in [1] is referred to throughout as the Green and Friedman model and is of particular relevance to this paper. They presented some analytical results for cases in which the equations simplify (e.g., when some of the anisotropic stress terms are negligible) but did not tackle the general case—a problem we pursue in this paper.

A number of studies have investigated transversely isotropic fluid flows in other geometries to gain insight into how their behavior is affected by the microstructure. These include studies of the stability of a transversely isotropic fluid in a Taylor-Couette device with the aim of understanding the behavior of suspensions of biomolecules, as well as treating the problem of Rayleigh-Bernard convection [24,25]. It was found in both works that transversely isotropic effects delay the onset of instabilities, primarily through the incorporation of an anisotropic shear viscosity. In the context of modifying transversely isotropic fluid models to incorporate active swimming suspensions, as in [2,26], transversely isotropic effects are also capable of increasing the size of a developing instability, in particular where translation diffusion is neglected. Other studies have focused on prototypical flows to give more generic insights into fluid-fiber interactions. For example, Phan-Thien and Graham studied both the flow of a transversely isotropic fluid around a sphere [27] and the squeezing flow of a layer of fluid compressed between two fixed plates [28] (this latter problem was studied independently for the case of an ideal fiber-reinforced fluid [11]).

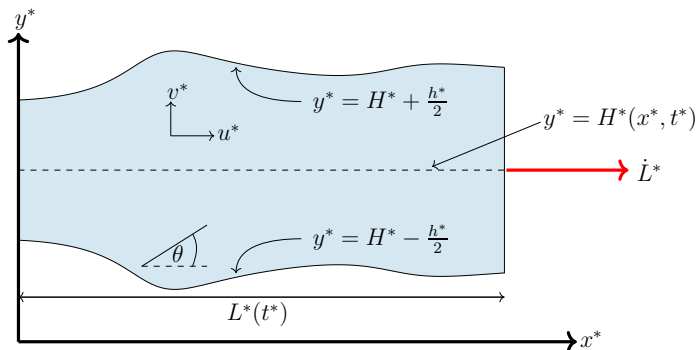


FIG. 1. Schematic of extensional flow of a sheet. The fluid is fixed to two plates at  $x^* = 0, L$ , by a no-slip boundary condition. The plate at  $x^* = L^*$  is moved at a prescribed speed  $\dot{L}^*$ . The center line of the fluid is given by  $H^*(x^*, t^*)$  and the thickness of the film by  $h^*(x^*, t^*)$ , so that the free boundaries of the film are located at  $y^* = H^* \pm \frac{h^*}{2}$ . Note that this figure is not to scale, as we model the thin film behavior of the sheet.

This paper uses a combination of analysis and numerical simulations to significantly extend the previous work of [1] to include cases where all of the anisotropic terms in the fluid stress are non-negligible, and the fiber alignment within the sheet may vary with depth. One issue of particular interest was to verify their conjecture that, in contrast to the Newtonian case, the center line of a transversely isotropic fluid sheet need not always be straight. As preliminary simulation of the model indeed produced results with nonflat center lines, we sought to confirm this prediction by additionally investigating the short timescale behavior of the sheet, similar to the work by [15,18] on the Newtonian problem.

The paper is organized as follows. In Sec. II we briefly recap the thin film approach and governing equations as given in [1], as well as introduce a short timescale. In order to present our solutions to the full Green and Friedman model, the equations are manipulated so that they become amenable to numerical strategies in Sec. III. We then present the arbitrary Lagrangian-Eulerian techniques we use to solve the model in Sec. IV and validate the numerical techniques by comparison with analytical results for short time, and we further present results primarily for a passive transversely isotropic fluid. In Sec. V we present results for the behavior of the fluid on a short timescale. We conclude with a discussion and suggestions for future work in Sec. VI.

## II. MATHEMATICAL MODEL

We consider the extensional flow of an inertialess thin sheet of incompressible, transversely isotropic, viscous fluid. As shown in Fig. 1, we use the 2D Cartesian coordinates  $(x^*, y^*)$  to describe the horizontal and vertical axis, respectively, with  $t^*$  denoting time (throughout this paper asterisks denote dimensional quantities). The upper and lower boundaries of the fluid sheet are denoted by  $y^* = H^\pm = H^* \pm \frac{h^*}{2}$ , where  $H^*(x^*, t^*)$  is the position of the center line and  $h^*(x^*, t^*)$  is the thickness of the fluid sheet. The left- and right-hand side boundaries are given by  $x^* = 0, L^*(t^*)$ . The right-hand side of the sheet, at  $x^* = L^*$ , is pulled in the  $x^*$  direction; we prescribe either the speed of pulling,  $\dot{L}^*$ , or the tension,  $T^*$ , applied to the sheet.

We let  $\mathbf{u}^* = (u^*, v^*)$  be the fluid velocities in the  $x^*, y^*$  directions, respectively, and denote the stress tensor by  $\sigma^*$ . The equations of conservation of fluid mass and momentum are thus

$$\nabla^* \cdot \mathbf{u}^* = 0, \quad (2.1)$$

$$\nabla^* \cdot \sigma^* = 0. \quad (2.2)$$

The constitutive law for  $\sigma^*$  is

$$\sigma_{ij}^* = -p^* \delta_{ij} + 2\mu^* e_{ij}^* + \mu_1^* a_i a_j + \mu_2^* a_i a_j a_k a_l e_{kl}^* + 2\mu_3^* (a_i a_l e_{jl}^* + a_j a_m e_{mi}^*), \quad (2.3)$$

where  $p^*$  is the pressure,  $\mathbf{a}$  is a unit vector describing the orientation of the fibers within the fluid, and  $\mathbf{e}^*$  is the rate of strain tensor. This relationship was derived by Ericksen [5] as the most general stress tensor that is linear in the rate of strain tensor  $\mathbf{e}^*$ , invariant under the transformation  $-\mathbf{a} \rightarrow \mathbf{a}$ , and satisfies  $\sigma^* = \sigma^{*T}$ . The constants  $\mu^*$ ,  $\mu_2^*$ ,  $\mu_3^*$ , are all viscosity-like parameters and  $\mu_1^*$  is the active tension in the fiber direction [1,23,29]. In the context of suspensions,  $\mu_1^*$  has been interpreted to model the contributions to stress caused by the active behavior of suspended particles [26].

We note first that by setting  $\mu_1^* = \mu_2^* = \mu_3^* = 0$ , one immediately recovers the stress tensor for an incompressible, isotropic Newtonian fluid, with  $\mu^*$  as the familiar dynamic (shear) viscosity. The physical interpretations of  $\mu_2^*$  and  $\mu_3^*$  can be identified by considering three deformations of a 2D sheet of fibers in a Cartesian plane, as illustrated in [1,9,24]. In the same way as previous work, we interpret  $\mu_2^*$  as the anisotropic extensional viscosity, and  $\mu_3^*$  the anisotropic shear viscosity. For the case of a dilute suspension of ellipsoidal particles, Holloway *et al.* [26] were able to give relations for  $\mu^*$ ,  $\mu_2^*$ , and  $\mu_3^*$  in terms of the solvent viscosity, particle volume fraction, and aspect ratio. Similarly, asymptotic values (in terms of the particle volume fraction and aspect ratio) were given for rodlike, disklike, and nearly spherical particles by Phan-Tien and Graham [28]. However, as far as we are aware, the accuracy of these predictions have never been tested against experimental results for any type of transversely isotropic fluid-fiber suspension. Finally, we observe that there is no velocity component to the  $\mu_1^*$  term, indicating that there exists stress in the fluid even when at rest and that this stress must be a tensile stress as no stress is induced in the fibers when the fluid is compressed.

In addition to the constitutive law for  $\sigma^*$ , we require an equation governing the evolution of the fiber direction. We use the form given by Green and Friedman (for derivation, see [1]), which results from allowing the fibers to advect with the fluid flow

$$\frac{\partial \mathbf{a}}{\partial t^*} + (\mathbf{u}^* \cdot \nabla^*) \mathbf{a} + \zeta^* \mathbf{a} = (\mathbf{a} \cdot \nabla^*) \mathbf{u}^*, \quad (2.4)$$

where

$$\zeta^*(x^*, y^*, t^*) = \mathbf{a} \cdot (\mathbf{a} \cdot \nabla^* \mathbf{u}^*) \quad (2.5)$$

is the fractional rate of extension of the fibers. The first two terms are the convective derivative of the fiber orientation, and the third is the fractional rate of extension of the fiber in the direction of the fibers, all of which balance with the effect of the fibers upon the flow velocity field on the right-hand side. Equation (2.4) corresponds to the specific case of Ericksen's equation in the long fiber limit [1,2,5]. Since  $\mathbf{a}$  is a unit vector and our model is 2D we write  $\mathbf{a} = (\cos \theta, \sin \theta)$ , where  $\theta(x^*, y^*, t^*)$  is the angle the fiber direction makes with the  $x^*$  axis.

In order to close the model, we must impose suitable boundary and initial conditions. At the ends of the sheet, we set

$$\begin{aligned} u^*(0, y^*, t^*) &= 0, & u^*(L^*, y^*, t^*) &= \dot{L}^*, \\ H^*(0, t^*) &= 0, & H^*(L^*, t^*) &= 0. \end{aligned}$$

On the upper and lower free surfaces, we apply a no-stress boundary condition

$$\sigma^* \cdot \hat{\mathbf{n}} = 0 \quad \text{on } y^* = H^* \pm \frac{1}{2} h^*,$$

together with the usual kinematic condition

$$v^* = \frac{\partial H^*}{\partial t^*} \pm \frac{1}{2} \frac{\partial h^*}{\partial t^*} + u^* \left( \frac{\partial H^*}{\partial x^*} \pm \frac{1}{2} \frac{\partial h^*}{\partial x^*} \right) \quad \text{on } y^* = H^* \pm \frac{1}{2} h^*. \quad (2.6)$$

Initial conditions must also be prescribed, however, since the number of initial conditions required depends upon the timescale considered; this will be discussed later.

### A. Thin film approximation

We now introduce the assumption that the sheet is thin, which allows considerable simplification of the governing equations. Full details of the derivation can be found in [1], but for the sake of completeness, we recapitulate the main points here and give the model equations in full in Appendix A. We let  $L_0$  and  $h_0$  be the initial length and typical initial thickness of the fluid sheet, respectively, and let  $U$  be a typical value for the velocity of the fluid at the pulled boundary. We then introduce the parameter  $\varepsilon = h_0/L_0 \ll 1$ , which is the initial inverse aspect ratio of the sheet. We are interested in the behavior of the sheet as it undergoes significant changes in length, and so consider the timescale  $t^* \sim L_0/U$ . Following [1,19] we nondimensionalize as follows:

$$(x^*, y^*) = (xL_0, \varepsilon yL_0), \quad (u^*, v^*) = (uU, \varepsilon vU), \quad p^* = \frac{\mu^*U}{L_0} p, \quad t^* = \frac{L_0}{U} t,$$

$$(H^*, L^*, h^*) = (\varepsilon L_0 H, L_0 L, \varepsilon L_0 h).$$

These scalings introduce the dimensionless material parameters

$$\mu_1 = \frac{\mu_1^* L}{\mu^* U}, \quad \mu_2 = \frac{\mu_2^*}{\mu^*}, \quad \mu_3 = \frac{\mu_3^*}{\mu^*}.$$

At this point, we exploit the thin geometry of the sheet by expanding all of the dependent variables as power series in terms of the inverse aspect ratio  $\varepsilon$ ,

$$u = u^{(0)} + \varepsilon u^{(1)} + \dots$$

with similar expressions for the other dependent variables (here, unlike in Howell [19], we encounter terms involving odd powers of  $\varepsilon$ ). After some lengthy algebra, full details of which are given in [1], we obtain a system of one-dimensional equations for the quantities  $h^{(0)}$ ,  $H^{(0)}$ ,  $u^{(0)}$ ,  $u^{(1)}$ ,  $v^{(0)}$ ,  $\theta^{(0)}$ . As a consequence of the analysis, it is found that the leading order longitudinal velocity satisfies  $u^{(0)} = u^{(0)}(x, t)$  only (i.e., the flow is extensional). Conservation of mass yields

$$\frac{\partial h^{(0)}}{\partial t} + \frac{\partial}{\partial x}(h^{(0)}u^{(0)}) = 0. \quad (2.7)$$

Taking a depth-averaged force balance over the sheet leads to the following equation for  $u^{(0)}$ :

$$\frac{\partial}{\partial x} \int_{H^{(0)-}}^{H^{(0)+}} 4(1 + \mu_3) \frac{\partial u^{(0)}}{\partial x} + \mu_1 \cos 2\theta^{(0)} + \mu_2 \left( \cos^2 2\theta^{(0)} \frac{\partial u^{(0)}}{\partial x} + \frac{1}{4} \sin 4\theta^{(0)} \frac{\partial u^{(1)}}{\partial y} \right) dy = 0. \quad (2.8)$$

In the case of prescribing an applied tension,  $T(t)$ , to the ends of the sheet in place of  $L(t)$ , taking the first integral of Eq. (2.8) equals this tension in the same way as the Newtonian Trouton model [19]. Consideration of the momentum equations and associated no-stress boundary conditions on the upper and lower boundaries of the fluid at higher order gives an equation governing the center line of the fluid,  $H^{(0)}$ :

$$\frac{\partial}{\partial x} \int_{H^{(0)-}}^{H^{(0)+}} \frac{\partial}{\partial x} \int_{H^{(0)-}}^y 4(1 + \mu_3) \frac{\partial u^{(0)}}{\partial x} + \mu_1 \cos 2\theta^{(0)} + \mu_2 \left( \cos^2 2\theta^{(0)} \frac{\partial u^{(0)}}{\partial x} + \frac{1}{4} \sin 4\theta^{(0)} \frac{\partial u^{(1)}}{\partial y} \right) ds dy = 0. \quad (2.9)$$

We note first that  $s$  is a dummy variable, and we are integrating over the second argument of the functions in the integrand twice, so that the quantities in the integrand of Eq. (2.9) are  $\theta^{(0)}(x, s, t)$ ,  $u^{(1)}(x, s, t)$ , and  $u^{(0)}(x, t)$  (to emphasize this, the dummy variable is not used in [1]). Additionally, we note that Eq. (2.9) is a particularly unusual form of an integro-differential equation,

wherein one of the variables of integration appears in the limit of one of the integrals. Equation (2.4) yields

$$\frac{\partial \theta^{(0)}}{\partial t} + u^{(0)} \frac{\partial \theta^{(0)}}{\partial x} + v^{(0)} \frac{\partial \theta^{(0)}}{\partial y} = -2 \sin \theta^{(0)} \cos \theta^{(0)} \frac{\partial u^{(0)}}{\partial x} - \sin^2 \theta^{(0)} \frac{\partial u^{(1)}}{\partial y}, \quad (2.10)$$

as an evolution equation governing the behavior of the fiber director field. The leading order transverse velocity is found by integrating the incompressibility condition and applying the kinematic condition (2.6)

$$v^{(0)} = \frac{\partial H^{(0)}}{\partial t} + \frac{\partial}{\partial x} (H^{(0)} u^{(0)}) - y \frac{\partial u^{(0)}}{\partial x}, \quad (2.11)$$

consideration of the  $x$ -momentum equation at  $\mathcal{O}(\varepsilon)$  with its associated boundary condition supplies

$$\frac{\partial u^{(1)}}{\partial y} = -\mu_1 \frac{2 \sin 2\theta^{(0)}}{4 + 4\mu_3 + \mu_2 \sin^2 2\theta^{(0)}} - \mu_2 \frac{\sin 4\theta^{(0)}}{4 + 4\mu_3 + \mu_2 \sin^2 2\theta^{(0)}} \frac{\partial u^{(0)}}{\partial x}, \quad (2.12)$$

as the next-order correction term for  $u$ . In this form, one can observe that in the case of  $\mu_1 = \mu_2 = \mu_3 = 0$ , we return to the Trouton model for a Newtonian fluid. In the case of  $\mu_1 = \mu_2 = 0$ , the fluid behaves very similarly to a Newtonian fluid, with the only modification being a modified Trouton ratio, which effectively only changes the tension required to be applied to the sheet to achieve the same behavior as a Newtonian fluid. In these cases, the model can be solved by means of a Lagrangian transformation, as detailed in [1, 19].

The boundary conditions for the leading order longitudinal velocity are then

$$u^{(0)}(0, t) = 0, \quad u^{(0)}(L, t) = \dot{L}. \quad (2.13)$$

We assume that the sheet is being extended in the  $x$  direction and that the end points of the center line remain fixed to  $y = 0$ , thus

$$H^{(0)}(0, t) = H^{(0)}(L, t) = 0. \quad (2.14)$$

The kinematic boundary condition yields

$$v^{(0)} = \frac{\partial H^{(0)}}{\partial t} \pm \frac{1}{2} \frac{\partial h^{(0)}}{\partial t} + u^{(0)} \left( \frac{\partial H^{(0)}}{\partial x} \pm \frac{1}{2} \frac{\partial h^{(0)}}{\partial x} \right) \quad \text{on } y = H^{(0)} \pm \frac{1}{2} h^{(0)}. \quad (2.15)$$

We will need to prescribe initial conditions for the thickness,  $h^{(0)}$ , and the fiber direction,  $\theta^{(0)}$ , in the sheet. As in the Newtonian problem (see [19]), we do not need to prescribe an initial condition for  $H^{(0)}$  as we are unable to satisfy an arbitrary initial condition for  $H^{(0)}$ , as noted in [1]. In order to study the behavior of sheets that do not initially obey Eq. (2.9) we must consider a shorter timescale than  $\frac{L_0}{U}$ . We turn to such a timescale in the next subsection.

## B. Short timescale model

Similarly to the Newtonian problem, we have a singular perturbation problem for  $H^{(0)}$  in  $t$ , the outer solution of which is determined by the solution of (2.9). As suspected by Green and Friedman [1], we discover that the center line is not necessarily straight (unlike the Newtonian case). In order to study the evolution of a sheet with an arbitrary initial condition for  $H^{(0)}$ , we follow a similar approach to Howell and Buckmaster *et al.* [18, 19] by considering a timescale of  $\varepsilon^2 \frac{L_0}{U}$ .

We note from (2.15), that in addition to rescaling time, we must also rescale the velocity  $v$ ; hence, we introduce

$$\tau = \frac{t}{\varepsilon^2}, \quad v = \frac{V}{\varepsilon^2}. \quad (2.16)$$

As in the previous section, we exploit the slender geometry of the sheet by expanding variables as a power series of  $\varepsilon$ . At leading order the continuity equation gives

$$\frac{\partial V^{(0)}}{\partial y} = 0, \quad (2.17)$$

which, combined with the kinematic condition at the same order

$$V^{(0)} = \frac{\partial H^{(0)}}{\partial \tau} \pm \frac{1}{2} \frac{\partial h^{(0)}}{\partial \tau} \quad \text{on } y = H^{\pm}, \quad (2.18)$$

gives

$$V^{(0)} = \frac{\partial H^{(0)}}{\partial \tau}, \quad \frac{\partial h^{(0)}}{\partial \tau} = 0, \quad (2.19)$$

since if  $V^{(0)}$  is independent of  $y$ , it must take the same value on the upper and lower free surfaces. Hence, we have an expression for  $V^{(0)}$  in terms of  $H^{(0)}$ , and note that there is no thinning of the sheet on this timescale. Additionally we obtain the equation for  $\theta^{(0)}$ ,

$$\frac{\partial \theta^{(0)}}{\partial \tau} + \frac{\partial H^{(0)}}{\partial \tau} \frac{\partial \theta^{(0)}}{\partial y} = 0. \quad (2.20)$$

Consideration of the  $x$ -momentum equation and the associated no-stress boundary condition at  $\mathcal{O}(\varepsilon)$  yields a result for  $u^{(0)}$ :

$$u^{(0)} = \bar{u}(x, \tau) + (H^{(0)} - y) \frac{\partial^2 H^{(0)}}{\partial \tau \partial x}, \quad (2.21)$$

where  $\bar{u}(x, t)$  is an as yet unknown function arising from integration. This is precisely the same result as for a Newtonian fluid [19]. Consideration of the  $y$ -momentum equation at the same order yields an identity which is already satisfied. Next, the  $y$ -momentum equation at  $\mathcal{O}(\varepsilon^2)$  yields an expression for pressure

$$\begin{aligned} & -\frac{\partial p^{(0)}}{\partial y} + \frac{\partial^2 V^{(0)}}{\partial x^2} + \frac{\partial^2 V^{(2)}}{\partial y^2} + \mu_1 \frac{\partial}{\partial y} (\sin^2 \theta^{(0)}) + \mu_2 \frac{\partial}{\partial y} \left[ \sin^2 \theta^{(0)} \cos^2 \theta^{(0)} \frac{\partial u^{(0)}}{\partial x} \right. \\ & \quad \left. + \cos \theta^{(0)} \sin^3 \theta^{(0)} \left( \frac{\partial u^{(1)}}{\partial y} + \frac{\partial V^{(1)}}{\partial x} \right) + \sin^4 \theta \frac{\partial V^{(2)}}{\partial y} \right] \\ & \quad + 2\mu_3 \frac{\partial}{\partial y} \left[ 2 \sin^2 \theta^{(0)} \frac{\partial V^{(2)}}{\partial y} + \cos \theta^{(0)} \sin \theta^{(0)} \left( \frac{\partial u^{(1)}}{\partial y} + \frac{\partial V^{(1)}}{\partial x} \right) \right] = 0, \end{aligned} \quad (2.22)$$

with the associated boundary condition

$$\begin{aligned} & -p^{(0)} + 2 \frac{\partial V^{(2)}}{\partial y} + \mu_1 \sin^2 \theta^{(0)} + \mu_2 \left[ \sin^2 \theta^{(0)} \cos^2 \theta^{(0)} \frac{\partial u^{(0)}}{\partial x} \right. \\ & \quad \left. + \cos \theta^{(0)} \sin^3 \theta^{(0)} \left( \frac{\partial u^{(1)}}{\partial y} + \frac{\partial V^{(1)}}{\partial x} \right) + \sin^4 \theta \frac{\partial V^{(2)}}{\partial y} \right] \\ & \quad + 2\mu_3 \left[ 2 \sin^2 \theta^{(0)} \frac{\partial V^{(2)}}{\partial y} + \sin \theta^{(0)} \cos \theta^{(0)} \left( \frac{\partial u^{(1)}}{\partial y} + \frac{\partial V^{(1)}}{\partial x} \right) \right] = 0 \quad \text{on } y = H^{(0)\pm}. \end{aligned} \quad (2.23)$$

A number of terms involving  $H^{(1)}$  arise in the calculation of (2.23), these terms are multiplied by a term that is identically zero and are thus omitted. We can directly integrate (2.22) and apply (2.23)

to obtain an equation for pressure

$$\begin{aligned}
 p^{(0)} = & -2 \frac{\partial u^{(0)}}{\partial x} + \mu_1 \sin^2 \theta^{(0)} + \mu_2 \left[ \sin^2 \theta^{(0)} \cos^2 \theta^{(0)} \frac{\partial u^{(0)}}{\partial x} + \cos \theta^{(0)} \sin^3 \theta^{(0)} \left( \frac{\partial u^{(1)}}{\partial y} + \frac{\partial V^{(1)}}{\partial x} \right) \right. \\
 & \left. - \sin^4 \theta \frac{\partial u^{(0)}}{\partial x} \right] + 2\mu_3 \left[ -2 \sin^2 \theta^{(0)} \frac{\partial u^{(0)}}{\partial x} + \sin \theta^{(0)} \cos \theta^{(0)} \left( \frac{\partial u^{(1)}}{\partial y} + \frac{\partial V^{(1)}}{\partial x} \right) \right], \quad (2.24)
 \end{aligned}$$

where  $\mathcal{O}(\varepsilon^2)$  continuity has been used to eliminate the  $V^{(2)}$  terms. This result for pressure is essentially a Newtonian pressure enhanced by the presence of the fibers; should we choose  $\mu_1 = \mu_2 = \mu_3 = 0$ , we recover the Newtonian pressure. We have also introduced  $u^{(1)}$  and  $V^{(1)}$  terms, which must now be eliminated. The  $\mathcal{O}(\varepsilon^2)$   $x$ -momentum equation is

$$\begin{aligned}
 \frac{\partial^2 u^{(1)}}{\partial y^2} + \mu_1 \frac{\partial}{\partial y} (\cos \theta^{(0)} \sin \theta^{(0)}) + \mu_2 \frac{\partial}{\partial y} \left[ \cos^3 \theta^{(0)} \sin^2 \theta^{(0)} \frac{\partial u^{(0)}}{\partial x} \right. \\
 \left. + \cos^2 \theta^{(0)} \sin^2 \theta^{(0)} \left( \frac{\partial u^{(1)}}{\partial y} + \frac{\partial V^{(1)}}{\partial x} \right) + \cos \theta^{(0)} \sin^3 \theta^{(0)} \frac{\partial V^{(2)}}{\partial y} \right] + \mu_3 \frac{\partial}{\partial y} \left( \frac{\partial u^{(1)}}{\partial y} + \frac{\partial V^{(1)}}{\partial x} \right) = 0, \quad (2.25)
 \end{aligned}$$

with the associated boundary condition

$$\begin{aligned}
 \frac{\partial u^{(1)}}{\partial y} + \frac{\partial V^{(1)}}{\partial x} + \mu_1 \cos \theta^{(0)} \sin \theta^{(0)} + \mu_2 \left[ \cos^3 \theta^{(0)} \sin^2 \theta^{(0)} \frac{\partial u^{(0)}}{\partial x} \right. \\
 \left. + \cos^2 \theta^{(0)} \sin^2 \theta^{(0)} \left( \frac{\partial u^{(1)}}{\partial y} + \frac{\partial V^{(1)}}{\partial x} \right) + \cos \theta^{(0)} \sin^3 \theta^{(0)} \frac{\partial V^{(2)}}{\partial y} \right] \\
 + \mu_3 \left( \frac{\partial u^{(1)}}{\partial y} + \frac{\partial V^{(1)}}{\partial x} \right) = 0, \quad \text{on } y = H^{(0)\pm}. \quad (2.26)
 \end{aligned}$$

Combining these yields the following compatibility condition:

$$\begin{aligned}
 \left( \frac{\partial u^{(1)}}{\partial y} + \frac{\partial V^{(1)}}{\partial x} \right) (1 + \mu_2 \cos^2 \theta^{(0)} \sin^2 \theta^{(0)} + \mu_3) + \mu_1 \cos \theta^{(0)} \sin \theta^{(0)} \\
 + \mu_2 \frac{\partial u^{(0)}}{\partial x} (\cos^3 \theta^{(0)} \sin \theta^{(0)} - \cos \theta^{(0)} \sin^3 \theta^{(0)}) = 0. \quad (2.27)
 \end{aligned}$$

We note that in the analysis, the terms  $V^{(1)}$ ,  $u^{(1)}$  only appear together. We can thus view (2.27) as an expression which allows us to eliminate both  $V^{(1)}$  and  $u^{(1)}$ . Hence, we can now write leading order pressure in terms of  $\theta^{(0)}$  and  $u^{(0)}$  only.

In order to close the model, we must go to yet higher orders in order to obtain equations for  $\bar{u}$  and  $H^{(0)}$ . Our approach is similar to Green and Friedman, [1]: we integrate the relevant equations over the depth of the sheet and apply the no-stress boundary conditions at  $y = H^{(0)\pm}$ . The expressions involved are rather cumbersome, but substituting for previously determined quantities produces considerable simplification; full details can be found in Appendix D. We finally obtain the following equation for  $\bar{u}$ :

$$\frac{\partial}{\partial x} \int_{H^{(0)-}}^{H^{(0)+}} \frac{\mu_1 \cos 2\theta^{(0)} + (4 + 4\mu_3 + \mu_2) \left[ \frac{\partial \bar{u}}{\partial x} + (H^{(0)} - y) \frac{\partial H^{(0)3}}{\partial x^2 \partial \tau} + \frac{\partial H^{(0)}}{\partial x} \frac{\partial^2 H^{(0)}}{\partial x \partial \tau} \right]}{4 + 4\mu_3 + \mu_2 \sin^2 2\theta^{(0)}} dy = 0. \quad (2.28)$$



The equation for  $H^{(0)}$  is

$$\begin{aligned} & \frac{\partial^2}{\partial x^2} \left( \int_{H^{(0)-}}^{H^{(0)+}} \int_{H^{(0)-}}^y \frac{\mu_1 \cos 2\theta^{(0)} + (4 + 4\mu_3 + \mu_2) \left[ \frac{\partial \bar{u}}{\partial x} + (H^{(0)} - y) \frac{\partial H^{(0)3}}{\partial x^2 \partial \tau} \right]}{4 + 4\mu_3 + \mu_2 \sin^2 2\theta^{(0)}} ds dy \right) \\ & = \frac{\partial}{\partial x^2} (H^{(0)+}) \left( \int_{H^{(0)-}}^{H^{(0)+}} \frac{\mu_1 \cos 2\theta^{(0)} + (4 + 4\mu_3 + \mu_2) \left[ \frac{\partial \bar{u}}{\partial x} + (H^{(0)} - y) \frac{\partial H^{(0)3}}{\partial x^2 \partial \tau} + \frac{\partial H^{(0)}}{\partial x} \frac{\partial^2 H^{(0)}}{\partial x \partial \tau} \right]}{4 + 4\mu_3 + \mu_2 \sin^2 2\theta^{(0)}} dy \right). \end{aligned} \quad (2.29)$$

We have now derived a system of equations for  $\theta^{(0)}$ ,  $\bar{u}$ , and  $H^{(0)}$ , namely, (2.20), (2.28), and (2.29), respectively. We note that (2.29) now includes a  $\frac{\partial^5 H^{(0)}}{\partial x^3 \partial \tau}$  term. We must prescribe two more boundary conditions for  $H^{(0)}$ , in addition to the those discussed in the previous section. We set

$$\frac{\partial H^{(0)}}{\partial x}(0, \tau) = \frac{\partial H^{(0)}}{\partial x}(L, \tau) = 0. \quad (2.30)$$

Much like the Green and Friedman model, Eqs. (2.20), (2.28), and (2.29) must be solved numerically. The numerical approach to the short timescale problem is more straightforward than that used for the Green and Friedman model (the details of which we will present in Sec. III).

### III. ARBITRARY LAGRANGIAN-EULERIAN METHODS

Although the Green and Friedman system, (2.7)–(2.12), and the short timescale system, (2.20) and (2.28)–(2.29), are both significant simplifications compared to the full 2D problem, they are too complex to allow significant analytical progress and must be solved numerically. In this section we reformulate the Green and Friedman and short-timescale equations into an arbitrary Lagrangian-Eulerian (ALE) formulation. ALE methods involve the construction of a reference domain together with mappings from this domain to both the Lagrangian and Eulerian descriptions of the flow. Unlike numerical techniques based on either a purely Lagrangian description, where the nodes of the computational mesh follow an associated material particle throughout the motion, or upon a purely Eulerian description, where the computational mesh is fixed and the motion of the continuum is with respect to the grid, ALE methods allow freedom in moving the mesh in a way that is not necessarily fixed to a material particle. This can provide accurate solutions when modeling greater distortions of a flow problem than can ordinarily be handled by numerical techniques upon a Lagrangian description, with more resolution than is often attainable by a purely Eulerian description [30].

Our approach largely follows [30], but we outline the details here for completeness. We introduce Lagrangian, Eulerian, and reference domain variables which we denote by  $\mathbf{X} = (X, Y)$ ,  $\mathbf{x} = (x, y)$ , and  $\mathbf{x}' = (x', y')$ , respectively. Converting between Eulerian and Lagrangian descriptions of flow fields is well established and has been employed in Newtonian extensional flow problems [1,19,31]. We define the map  $\varphi$  from the Lagrangian to the Eulerian descriptions such that

$$(\mathbf{x}, t) = (\varphi(\mathbf{X}, t), t),$$

where the material velocity  $\mathbf{v}$  is given by

$$\frac{\partial \varphi}{\partial t} = \mathbf{v}(\mathbf{X}, t), \quad (3.1)$$

so that the familiar material time derivative of an arbitrary scalar field (e.g., pressure) is

$$\frac{Df(\mathbf{X}, t)}{Dt} = \frac{\partial f(\mathbf{x}, t)}{\partial t} + \frac{\partial f(\mathbf{x}, t)}{\partial \mathbf{x}} \frac{\partial \varphi}{\partial t} = \frac{\partial f}{\partial t} + (\mathbf{v} \cdot \nabla_{\mathbf{x}})f. \quad (3.2)$$

Now, it remains only to define the map from the reference domain to the Eulerian domain, which we denote by  $\Phi$ . This satisfies

$$(\mathbf{x}, t) = (\Phi(\mathbf{x}', t), t).$$

The mesh velocity,  $\mathbf{u}_{\text{mesh}}$ , is given by

$$\mathbf{u}_{\text{mesh}}(\mathbf{x}', t) = \frac{\partial \Phi}{\partial t}.$$

We obtain the relations between physical quantities, such as pressure, in the reference and Eulerian descriptions in the same way we do between Lagrangian and Eulerian descriptions. In particular, the time derivative of an arbitrary scalar field  $f$  is

$$\frac{\partial f(\mathbf{x}', t)}{\partial t} = \frac{\partial f(\mathbf{x}, t)}{\partial t} + (\mathbf{u}_{\text{mesh}} \cdot \nabla_{\mathbf{x}})f, \quad (3.3)$$

so that the transformation from the reference to the Eulerian description behaves very much like a familiar transformation between Lagrangian and Eulerian frames. For convenience, we rewrite (3.3) as

$$\frac{\partial f(\mathbf{x}', t)}{\partial t} - \frac{\partial \mathbf{x}'}{\partial \mathbf{x}}(\mathbf{u}_{\text{mesh}} \cdot \nabla_{\mathbf{x}'})f = \frac{\partial f(\mathbf{x}, t)}{\partial t}. \quad (3.4)$$

As a final note, if  $\Phi = \varphi$ , then the reference description is the same as the Lagrangian description and thus  $\mathbf{u}_{\text{mesh}} = \mathbf{v}$ . If  $\Phi = \mathbf{x}'$ , then the reference description is the same as the Eulerian description, and  $\mathbf{u}_{\text{mesh}} = \mathbf{0}$ . For further explanation of ALE techniques, we direct the reader to [30].

### A. Employing ALE upon the Green and Friedman model

Henceforth we drop the superscript notation on leading order terms. We first employ ALE techniques upon the equations governing the  $t \sim \frac{L_0}{U}$  timescale, Eqs. (2.7)–(2.15). We define the reference domain,  $D_{\text{ref}}$ , to be

$$(x', y') \in D_{\text{ref}} = [0, 1] \times \left[-\frac{1}{2}, \frac{1}{2}\right]. \quad (3.5)$$

We define the mapping from the reference variables to the Eulerian variables  $\Phi : D_{\text{ref}} \rightarrow [0, L] \times [H^-, H^+]$  such that

$$(x, y) = \Phi(x', y') = \left[ Lx', H\left(\frac{Lx'}{L(0)}, t\right) + h\left(\frac{Lx'}{L(0)}, t\right)y' \right]. \quad (3.6)$$

This choice of map maintains equidistant spacing in the mesh in both horizontal and vertical directions. Therefore, our discretization of  $D_{\text{ref}}$  can be a simple equidistant grid. As already discussed, the mesh velocity is readily obtained by differentiating the mapping  $\Phi$  with respect to time. Written in terms of Eulerian variables, we have

$$\frac{\partial \Phi}{\partial t} = \mathbf{u}_{\text{mesh}} = \left\{ \dot{L} \frac{x}{L}, \dot{L} \frac{x}{L} \left[ \frac{\partial H}{\partial x}(x, t) + \frac{y - H(x, t)}{h(x, t)} \frac{\partial h}{\partial x}(x, t) \right] + \frac{\partial H}{\partial t}(x, t) + \frac{y - H(x, t)}{h(x, t)} \frac{\partial h}{\partial t}(x, t) \right\}. \quad (3.7)$$

We now account for the introduction of the moving mesh by using (3.4) and (3.6), we first modify the equation for  $\theta$ , (2.10). Using (2.12) to eliminate  $u^{(1)}$ , this equation becomes

$$\frac{\partial \theta}{\partial t} + \left( \frac{u - u_{\text{mesh}}}{L} \right) \frac{\partial \theta}{\partial x'} + \left( \frac{v - v_{\text{mesh}}}{h} \right) \frac{\partial \theta}{\partial y'} = \frac{\sin 2\theta \left[ 2\mu_1 \sin^2 \theta - \frac{1}{L} (1 + 2\mu_2 \sin^2 \theta) \frac{\partial u}{\partial x'} \right]}{4 + 4\mu_3 + \mu_2 \sin^2 2\theta}. \quad (3.8)$$

This form of (3.8) allows us yet further simplification. As explicitly demonstrated in Appendix B, this equation corresponds to advection purely in a horizontal direction on the reference domain, which significantly eases implementation. We note that this also decouples  $\theta$  from  $H$ , and since  $v$

does not arise in any other equation, we need not prescribe an initial  $H$  and can simply compute the transverse velocity on demand. To summarize the model in the ALE form, we have

$$\frac{\partial h}{\partial t} + \left( \frac{u - u_{\text{mesh}}}{L} \right) \frac{\partial h}{\partial x'} + \frac{1}{L} \frac{\partial u}{\partial x'} = 0, \quad (3.9)$$

$$\frac{\partial \theta}{\partial t} + \left( \frac{u - u_{\text{mesh}}}{L} \right) \frac{\partial \theta}{\partial x'} = \frac{\sin 2\theta (2\mu_1 \sin^2 \theta - \frac{1}{L} [4 + 4\mu_3 + 2\mu_2 \sin^2 \theta] \frac{\partial u}{\partial x'})}{4 + 4\mu_3 + \mu_2 \sin^2 2\theta}, \quad (3.10)$$

$$\frac{\partial}{\partial x'} \int_{-\frac{1}{2}}^{\frac{1}{2}} \frac{\mu_1 \cos 2\theta + \frac{1}{L} (4 + 4\mu_3 + \mu_2) \frac{\partial u}{\partial x'}}{4 + 4\mu_3 + \mu_2 \sin^2 2\theta} h dy' = 0, \quad (3.11)$$

$$\begin{aligned} \frac{\partial^2}{\partial x'^2} \int_{-\frac{1}{2}}^{\frac{1}{2}} \int_{-\frac{1}{2}}^{y'} \frac{\mu_1 \cos 2\theta + \frac{1}{L} (4 + 4\mu_3 + \mu_2) \frac{\partial u}{\partial x'}}{4 + 4\mu_3 + \mu_2 \sin^2 2\theta} h^2 ds' dy' \\ = \left( \frac{\partial^2 H}{\partial x'^2} + \frac{1}{2} \frac{\partial^2 h}{\partial x'^2} \right) \int_{-\frac{1}{2}}^{\frac{1}{2}} \frac{\mu_1 \cos 2\theta + \frac{1}{L} (4 + 4\mu_3 + \mu_2) \frac{\partial u}{\partial x'}}{4 + 4\mu_3 + \mu_2 \sin^2 2\theta} h dy', \end{aligned} \quad (3.12)$$

for  $(x', y') \in D_{\text{ref}}$ . The associated boundary and initial conditions now become

$$u(0, t) = 0, \quad u(1, t) = 1, \quad (3.13)$$

$$H(0, t) = 0, \quad H(1, t) = 0, \quad (3.14)$$

$$h(x', 0) = h_i(x'), \quad \theta(x', y', 0) = \theta_i(x', y'). \quad (3.15)$$

We exclude the equation for the transverse velocity  $v$ , since this quantity is readily calculated from (2.11) at any  $(x', y', t)$  once the model (3.9)–(3.12) is solved.

In order to solve this model we use the following algorithm. Given initial conditions, Eq. (3.11) is solved to obtain  $u(x', 0)$ , using the trapezoidal rule and a finite difference approximation. We note that this particular equation can be approached in either ALE or Eulerian variables, since applying the trapezoidal rule to solve the integral (3.11) effectively decouples  $H$  from the system (see Appendix C). Once solved, Eqs. (3.9) and (3.10) can be used to update  $h, \theta$  to the next time step, at which point the process is repeated until the required end time is reached. The quantities  $v, H$  can then be computed at any time using (2.11) and (3.12), respectively, as well as any other quantities of interest. In our implementation, we solved Eqs. (3.9)–(3.12) in the ALE form given above. Since the ALE framework acts like a simple substitution on the integral equations, it is equally possible to discretize and solve Eqs. (3.11) and (3.12) in their Eulerian forms, and indeed the discretization is similar. We include the discretizations of Eqs. (3.11) and (3.12) in Appendix C.

## B. Validation of numerical method

In order to validate the approach, we consider the early-time behavior of the sheet for which an analytical expression is available [1]. Introducing the short timescale  $t' = \delta^{-1}t$ , where  $\varepsilon \ll \delta \ll 1$ , assuming constant initial film thickness,  $h_i$ , and alignment angle,  $\theta_i$ , and performing a Taylor expansion on the variables so that

$$h = h_i + \hat{h}t'\delta + \mathcal{O}(\delta^2),$$

$$\theta = \theta_i + \hat{\theta}t'\delta + \mathcal{O}(\delta^2),$$

where  $\hat{h}, \hat{\theta}$  are the changes in thickness and fiber direction, respectively, it is possible to derive an analytical expression for the evolution of the fiber angle in the sheet for constant initial conditions

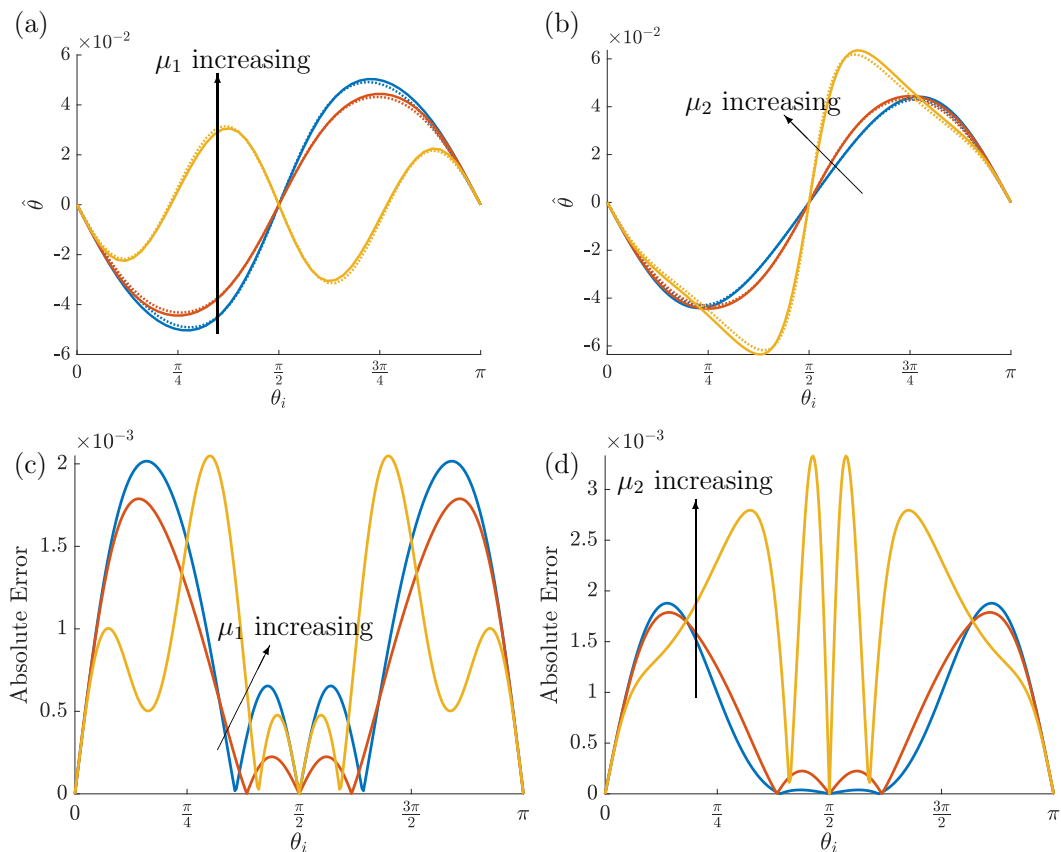


FIG. 2. Comparison of the analytical result for  $\hat{\theta}$  at  $t' = 0.05$ , with  $\theta_i \in [0, \pi]$  for a)  $\mu_1 = 0, 1, 10$  (blue, red, and yellow, respectively) with  $\mu_2 = \mu_3 = 1$  fixed and b)  $\mu_2 = 0, 1, 10$  (blue, red, and yellow, respectively) with  $\mu_1 = \mu_3 = 1$  fixed. The analytical results from (3.16) are solid lines; the dotted lines are numerical results obtained by solving (3.9)–(3.12). The absolute errors between the numerical and analytical results are given for (c) varied  $\mu_1$  and (d) varied  $\mu_2$ , with step sizes given by  $\Delta x = 0.0033$ ,  $\Delta t' = 0.000167$ .

for thickness and fiber direction; see [1]. The result is

$$\hat{\theta} = -2 \sin 2\theta_i + \frac{2 \sin^2 \theta_i}{4 + 4\mu_3 + \mu_2 \sin^2 2\theta_i} \left( \mu_1 \sin 2\theta_i + \frac{\mu_2}{2} \sin 4\theta_i \right), \quad (3.16)$$

where  $t'\hat{\theta}$  is the total change in the fiber angle over the short time  $\tau$ , and  $\theta_i$  is the constant initial condition. In [1], the authors note that a consequence of this analysis is that so long as  $\mu_1, \mu_2, T$  are all sufficiently small, the fibers will align with the direction of pulling as long as  $\theta_i \neq \frac{\pi}{2}, \frac{3\pi}{2}$ . In Fig. 2 we plot the numerical solution of (3.9)–(3.12) against Eq. (3.16) up to  $t' = 0.05$ . The maximum absolute error in Fig. 2(b) is 0.0033 and occurs at  $\theta_i = 1.4556, 1.6860$ , for  $\mu_2 = 10$ .

### C. Employing ALE to the short timescale

We again define the reference domain and mapping from the reference to the Eulerian domain by (3.5) and (3.6). In Sec. II B we determined that on the short timescale there is no extension or

thinning of the sheet, which gives the simpler mesh velocity

$$\mathbf{u}_{\text{mesh}} = \left( 0, \frac{\partial H}{\partial t}(x, t) \right). \quad (3.17)$$

The fiber director equation on the short timescale (2.20) becomes

$$\frac{\partial \theta}{\partial \tau} = 0, \quad (3.18)$$

hence there is no evolution in  $\theta$  in the ALE framework on this timescale. Next, Eq. (2.28) gives

$$\begin{aligned} & \frac{\partial}{\partial x'} \int_{-\frac{1}{2}}^{\frac{1}{2}} \frac{\mu_1 \cos 2\theta + (4 + 4\mu_3 + \mu_2) \frac{\partial \bar{u}}{\partial x'}}{4 + 4\mu_3 + \mu_2 \sin^2 2\theta} h dy' + \frac{1}{L} \frac{\partial}{\partial x'} \left( \frac{\partial H}{\partial x'} \frac{\partial^2 H}{\partial x' \partial \tau} \int_{-\frac{1}{2}}^{\frac{1}{2}} \frac{(4 + 4\mu_3 + \mu_2)}{4 + 4\mu_3 + \mu_2 \sin^2 2\theta} h dy' \right. \\ & \left. - \frac{\partial^3 H}{\partial x'^2 \partial \tau} \int_{-\frac{1}{2}}^{\frac{1}{2}} \frac{(4 + 4\mu_3 + \mu_2) y'}{4 + 4\mu_3 + \mu_2 \sin^2 2\theta} h^2 dy' \right) = 0, \end{aligned} \quad (3.19)$$

with the momentum equation (2.29) becoming

$$\begin{aligned} & \frac{\partial^2}{\partial x'^2} \left( \int_{-\frac{1}{2}}^{\frac{1}{2}} \int_{-\frac{1}{2}}^{\frac{1}{2}} \frac{\mu_1 \cos 2\theta + (4 + 4\mu_3 + \mu_2) \frac{1}{L} \frac{\partial \bar{u}}{\partial x'}}{4 + 4\mu_3 + \mu_2 \sin^2 2\theta} h^2 d\tilde{y}' d\tilde{y} + \frac{\partial H}{\partial x'} \frac{\partial^2 H}{\partial x' \partial \tau} \right. \\ & \left. \times \int_{-\frac{1}{2}}^{\frac{1}{2}} \int_{-\frac{1}{2}}^{\frac{1}{2}} \frac{4 + 4\mu_3 + \mu_2}{4 + \mu_3 + \mu_2 \sin^2 2\theta} h^2 d\tilde{y}' d\tilde{y} - \frac{\partial^3 H}{\partial x'^2 \partial \tau} \int_{-\frac{1}{2}}^{\frac{1}{2}} \int_{-\frac{1}{2}}^{\frac{1}{2}} \frac{(4 + 4\mu_3 + \mu_2) \tilde{y}'}{4 + 4\mu_3 + \mu_2 \sin^2 2\theta} h^3 d\tilde{y}' d\tilde{y} \right) \\ & = \left( \frac{\partial^2 H}{\partial x'^2} + \frac{1}{2} \frac{\partial^2 h}{\partial x'^2} \right) \left( \int_{-\frac{1}{2}}^{\frac{1}{2}} \frac{\mu_1 \cos 2\theta + (4 + 4\mu_3 + \mu_2) \frac{1}{L} \frac{\partial \bar{u}}{\partial x'}}{4 + 4\mu_3 + \mu_2 \sin^2 2\theta} h d\tilde{y} \right. \\ & \left. + \frac{\partial H}{\partial x'} \frac{\partial^2 H}{\partial x' \partial \tau} \int_{-\frac{1}{2}}^{\frac{1}{2}} \frac{4 + 4\mu_3 + \mu_2}{4 + 4\mu_2 + \mu_2 \sin^2 2\theta} h d\tilde{y} - \frac{\partial^3 H}{\partial x'^2 \partial \tau} \int_{-\frac{1}{2}}^{\frac{1}{2}} \frac{(4 + 4\mu_3 + \mu_2) \tilde{y}}{4 + 4\mu_3 + \mu_2 \sin^2 2\theta} h^2 d\tilde{y} \right). \end{aligned} \quad (3.20)$$

As the equation for  $\theta$ , (3.18), shows that there is no evolution of  $\theta$  in the ALE framework, we now need only to solve (3.19) and (3.20) for  $\bar{u}$  and  $H$ , respectively. As  $\frac{\partial \bar{u}}{\partial x}$  depends on only  $x'$ ,  $\tau$ , it can be removed from the integrals, the integral coefficients are precomputable at each time step, which significantly eases the numerical implementation.

The strategy is as follows: given an initial condition for  $\theta, H$ , we simultaneously solve for  $\bar{u}$  at the current time step, and  $H$  at the next time step using a forward time-centered space finite difference discretization. We repeat this until we reach the desired time. We give the discretizations of Eqs. (2.20), (3.19), and (3.20) and details of the construction of the resulting linear system in Appendix E.

#### IV. RESULTS ON THE EXTENSIONAL FLOW TIMESCALE

We first examine the behaviors of the sheet on the  $t \sim \frac{L_0}{U}$  timescale. Green and Friedman considered special cases where further analytical insight into the behavior of the model is possible. They considered two cases: where the sheet is not extending ( $\dot{L} = 0$ ), in which the fibers tend to align parallel to the  $y$  axis, and the case of an extensional flow with  $\mu_1 = \mu_2 = 0$ . In the second case, the equations imply that  $H \equiv 0$  and are amenable to further progress via Lagrangian transformation. It is found that the fibers align with the direction of extension (i.e., parallel to the  $x$  axis) [1]. Throughout the next section we assume that  $\mu_1 = 0$  in order to examine the contributions of the anisotropic viscosities  $\mu_2, \mu_3$  to the behavior of the sheet.

**A. Solutions for initially uniform transversely isotropic sheets with  $\mu_1 = 0$** 

We now aim to study the effect of the anisotropic viscosities  $\mu_2, \mu_3$  upon the fluid as the sheet is stretched. We first turn our attention to transversely isotropic sheets that have an initially constant thickness and  $\mu_1 = 0$ . For clarity of exposition, we introduce the quantity

$$G(x', y', t) = hG_1 + \frac{h}{L} \frac{\partial u}{\partial x'} G_2 = \int_{-\frac{1}{2}}^{y'} \frac{\mu_1 \cos 2\theta + (4 + 4\mu_3 + \mu_2) \frac{1}{L} \frac{\partial u}{\partial x'} h}{4 + 4\mu_3 + \mu_2 \sin^2 2\theta} dy', \quad (4.1)$$

so that

$$G_1(x', y', t) = \int_{-\frac{1}{2}}^{y'} \frac{\mu_1 \cos 2\theta}{4 + 4\mu_3 + \mu_2 \sin^2 2\theta} dy', \quad (4.2)$$

$$G_2(x', y', t) = \int_{-\frac{1}{2}}^{y'} \frac{(4 + 4\mu_3 + \mu_2)}{4 + 4\mu_3 + \mu_2 \sin^2 2\theta} dy'. \quad (4.3)$$

The definitions of  $G_1$  and  $G_2$  are readily obtained in the physical domain by performing the inverse of the transformation  $\Phi$  and reintroducing dimensional parameters. We start by considering sheets with no tension in the fiber direction when the fluid is at rest, that is,  $\mu_1 = 0$ , in which case the equation for  $u$  in ALE variables (3.11) becomes

$$\frac{\partial}{\partial x'} \left[ h \frac{\partial u}{\partial x'} G_2 \left( x', \frac{1}{2}, t \right) \right] = 0. \quad (4.4)$$

This is of the same form as the longitudinal momentum equation in the Trouton model, with  $G_2$  playing the role of a spatially varying viscosity (setting  $\mu_2 = \mu_3 = 0$  gives  $G_2 = 4$ , the Trouton ratio for a Newtonian thin sheet [19]). We interpret  $G_2$  as a heterogeneous, time-dependent, ‘‘effective viscosity.’’ As we shall show, we see the effect of  $G_2$  is to induce ‘‘necking’’ in the sheet (the sheet undergoes thinning at a greater rate in some areas of the sheet than others, generating a ‘‘neck’’). This behavior has been observed in Newtonian fluids which possess an inhomogeneous viscosity.

We also note that if the fiber angle is independent of  $x'$ , or if  $\mu_1 = \mu_2 = 0$  [1], then  $G_2$  as it appears in Eq. (4.4) does not possess  $x'$  dependence. Hence, a fluid that does not possess tension in the fiber direction when at rest and has a uniform fiber direction will behave like a Newtonian fluid, with a modified viscosity. In this case, the center line of the fluid is always a straight line, and the model can be solved by transforming to Lagrangian variables, as detailed in [1, 19].

A first integral of (4.4) yields

$$h \frac{\partial u}{\partial x'} G_2 \left( x', \frac{1}{2}, t \right) = T(t), \quad (4.5)$$

where  $T$  is the tension applied to the sheet. Directly from (4.5) we see that  $G_2$  may induce nonlinear behaviors in  $u$ . For a Newtonian fluid, or a transversely isotropic fluid where only  $\mu_3 \neq 0$ , choosing an initial condition of constant thickness across the sheet yields that  $u$  must be linear in  $x'$ . In that case, as shown by Howell,  $u = \dot{L}x$  for all time, and  $h$  is a function of  $t$  only [19] (using a similar approach, the same result was shown for a fluid with  $\mu_1 = \mu_2 = 0$ , [1]). However, for a transversely isotropic sheet with  $\mu_2 \neq 0$ , the existence of the trigonometric terms inside  $G_2$  prohibits this. When  $\mu_2 > 0$ , with  $h(x', 0)$  constant, if  $\theta(x', y', 0)$  depends upon  $x'$ , this will result in  $u$  becoming nonlinear in  $x'$ , and by (3.9), this will cause  $h$  to become spatially nonuniform. In Fig. 3 we illustrate the early evolution of the thickness of the sheet and the behavior of  $1/G_2$ , for  $h(x', 0) = 1$ ,  $\theta(x', y', 0) = \cos(4\pi x' y') - 0.1$ ,  $\mu_1 = \mu_3 = 0$ ,  $\mu_2 = 5$ . Notice that the sheet thickness immediately becomes nonuniform, and the location of the peaks and troughs in  $1/G_2$  correlates with the locations of local minima and maxima of the thickness of the sheet when  $t \neq 0$ .

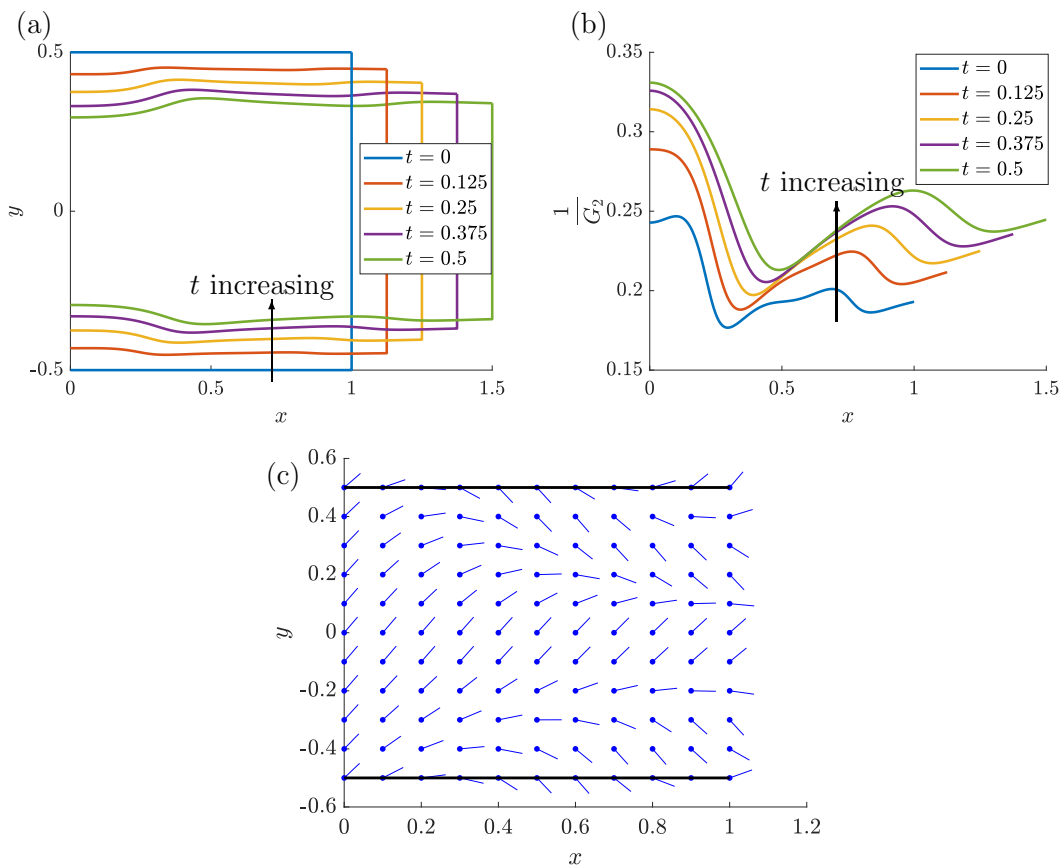


FIG. 3. Evolution of (a) the thickness of the sheet and (b) the function  $\frac{1}{G_2}$  at the times  $t = 0, 0.125, 0.25, 0.375, 0.5$ , pulling at  $L(t) = 1 + t$ , with the initial conditions  $\theta(x', y', 0) = \cos(4\pi x' y') - 0.1$  [plotted in (c)],  $h(x', 0) = 1$ , and parameter values  $\mu_1 = \mu_3 = 0, \mu_2 = 5$ .

### 1. Effect of varying the extensional and shear viscosities $\mu_2, \mu_3$ with $\mu_1 = 0$

In this section we continue to use the initial conditions  $h(x', 0) = 1, \theta(x', y', 0) = \cos(4\pi x' y') - 0.1, \mu_1 = 0$ , but now vary  $\mu_2$  and  $\mu_3$  and compare the state of the sheet at  $t = 5$ . First, we note that varying  $\mu_3$  with  $\mu_2 = 0$  simply changes the value of the constant obtained from  $G_2$ . We plot in Fig. 4 the thickness and velocity  $u$  in the sheet for varied  $\mu_2$  and notice that for these choices of  $\theta(x', y', 0)$  and  $h(x', 0)$  that we see a global increase in the longitudinal velocity for increasing  $\mu_2$ . Additionally, we see that there are regions of the sheet that thin more quickly for increasing  $\mu_2$ , and other regions that thin more slowly. Intuition based upon the behavior of a pipe flow would lead one to expect that in regions where the sheet is thicker, the velocity would be lower. This is not true here, and as in the previous subsection, this behavior is linked to the behavior of  $G_2$  as we shall now demonstrate. Integrating (4.5) and using that  $u(L) = 1$ , we may write

$$1 = T \int_0^L \frac{1}{h G_2(x', \frac{1}{2}, t)} dx'. \quad (4.6)$$

We note that by (4.3) and (4.6), as the fibers within the fluid sheet flatten out,  $G_2$  increases everywhere and hence so does the tension,  $T$ . In addition, the tension will increase with increasing

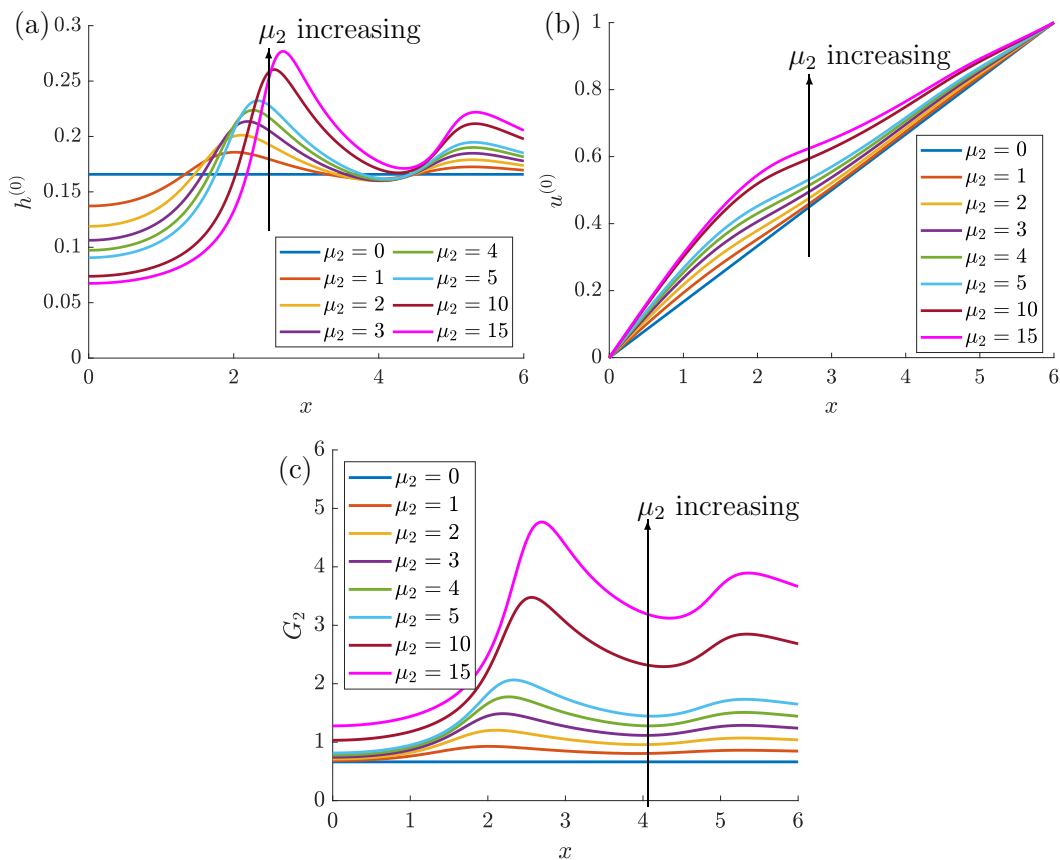


FIG. 4. Comparison of (a) thickness, (b) longitudinal velocity, and (c)  $G_2$  at  $t = 5$ , pulling with  $L(t) = 1 + t$ , for  $\mu_2 = 0, 1, 2, 3, 4, 5, 10, 15$ , with the conditions  $h(x', 0) = 1$ ,  $\theta(x', y', 0) = \cos(4\pi x' y') - 0.1$ ,  $\mu_1 = \mu_3 = 0$ . Notice that more extreme behavior in  $G_2$  correlates with greater change in the thickness and velocity profile across the sheet and increases with  $\mu_2$ .

$\mu_2$ . Eliminating tension from Eq. (4.6) gives a result for  $u$ ,

$$u = \frac{\int_0^{x'} \frac{1}{hG_2(s, \frac{1}{2}, t)} ds}{\int_0^L \frac{1}{hG_2(x', \frac{1}{2}, t)} dx'}, \quad (4.7)$$

and so  $u$  behaves as a cumulative integral. If  $G_2$  is fixed, the longitudinal velocity does behave as a pipe flow intuition would expect (in regions where  $h$  is small,  $1/h$  is large, and  $u$  will increase). However, when  $G_2$  is not fixed (i.e.,  $\mu_2 \neq 0$ ), the behavior of the longitudinal velocity is more complex. The derivative  $u_x$  is dependent on the behavior of  $hG_2$ . We see this in Fig. 4, where we give results for  $\mu_3 = 0$  and see that for increasing  $\mu_2$ ,  $hG_2$  decreases (despite the increase in  $G_2$ ), which leads to a greater  $u_x$  on the left-hand side of the domain. Where  $hG_2$  is larger, around  $x = 3$ , we see the gradient of  $u$  decrease below that of  $\mu_2 = 0$ .

If we allow  $\mu_2, \mu_3 \neq 0$ , we find that increasing  $\mu_3$  has the effect of globally increasing the value of  $G_2$  and hence the tension applied to the ends of the sheet and inhibits the uniformity-breaking behavior of  $\mu_2$ .

That is, increasing the  $\mu_3$  term drives the fluid to behave in a “more Newtonian” manner, albeit with a higher tension, while increasing  $\mu_2$  drives the non-Newtonian behavior of breaking the



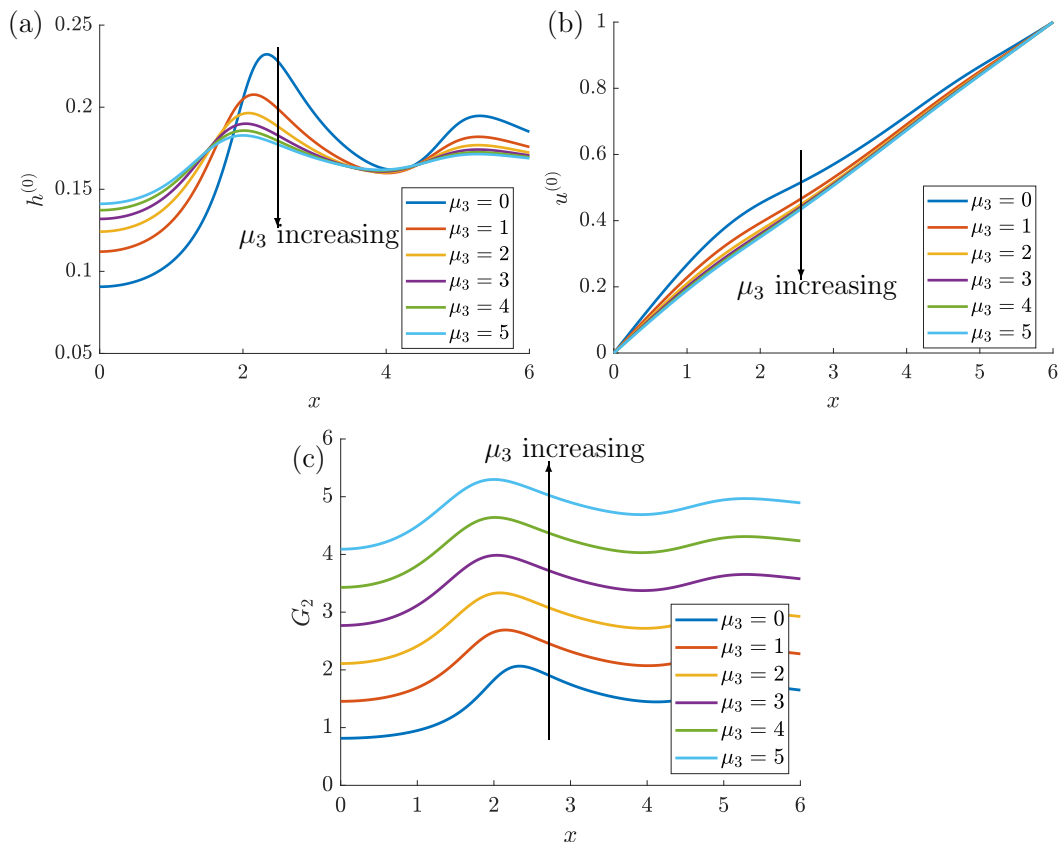


FIG. 5. Comparison of (a) thickness of the sheet, and (b) longitudinal velocity of the sheet at  $t = 5$  and (c)  $G_2$  at  $t = 5$ ,  $\theta(x', y', 0) = \cos(4\pi x' y') - 0.1$ , for  $\mu_1 = 0$ ,  $\mu_2 = 5$ , and  $\mu_3 = 0, 1, 2, 3, 4, 5$ .

uniformity of the sheet previously discussed. As an illustrative example, in Fig. 5 we plot the behavior of the sheet at  $t = 5$  for varying  $\mu_3$  with  $\mu_2 = 5$  and initial conditions  $h(x', 0) = 1$ ,  $\theta(x', y', 0) = \cos(4\pi x' y') - 0.1$ . Notice that increasing  $\mu_3$  causes the thickness of the sheet to exhibit less deviation from uniformity, and the longitudinal velocity to tend towards  $u = x'$ , the solution for a Newtonian fluid.

## B. Behavior of the fiber

### 1. Uniform initial fiber director field

We now turn our attention to the fiber behavior within the sheet. In [1] Green and Friedman considered two special cases that validate our results. It is found that for the case of an extensional flow with  $\mu_1, \mu_2 = 0$  the fibers align with the direction of extension (i.e., parallel to the  $x$  axis) and that for the special case of not extending the sheet ( $\dot{L} = 0$ ) with  $\mu_1, \mu_2, \mu_3 \neq 0$ , the fibers tend to align parallel to the  $y$  axis.

For  $\mu_1 = 0$ , we start by extending the results obtained for early time with a constant initial fiber direction described in Sec. 6 of Green and Friedman [1]. If  $h_i, \theta_i$  are uniform, then we can see from Eqs. (3.10) and (3.11) that  $\frac{\partial u}{\partial x'} = 1$ , and  $\theta$  and  $h$  must be functions of time only. Moreover, Eq. (3.10) yields

$$\frac{d\theta}{dt} = \frac{-\sin 2\theta(4 + 4\mu_3 + 2\mu_2 \sin^2 \theta)^{\frac{1}{L}}}{4 + 4\mu_3 + \mu_2 \sin^2 2\theta}, \quad (4.8)$$

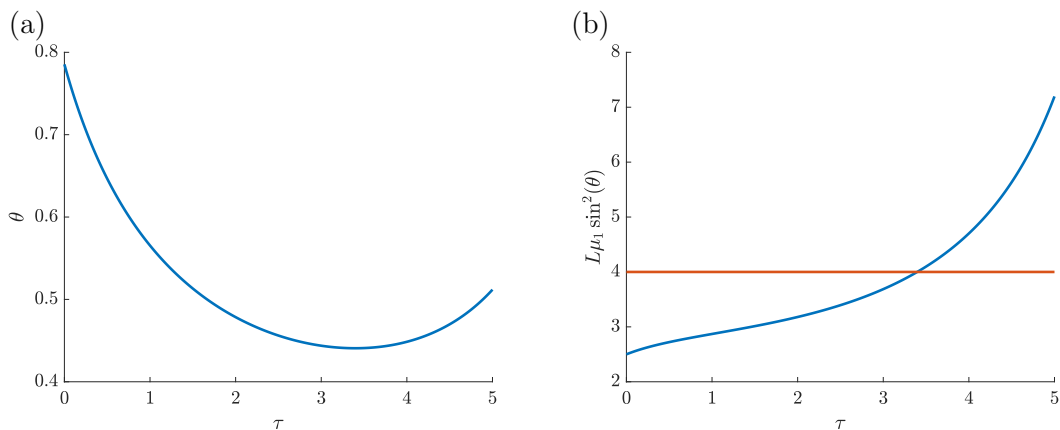


FIG. 6. Evolution of (a) the fiber angle  $\theta$  and (b) the left-hand side of (4.10) (blue), with the threshold  $2 + 2\mu_3$ , (red), for the choices of  $\theta_i = \frac{\pi}{4}$ ,  $L_i = h_i = 1$ ,  $\mu_1 = 5$ ,  $\mu_2 = 0$ ,  $\mu_3 = 1$ . Note the reversal in the direction of rotation when  $L\mu_1 \sin^2 \theta \geq 2 + 2\mu_3$ .

which implies that the behavior of the fibers is determined by the sign of  $\sin 2\theta$ . For  $0 < \theta < \frac{\pi}{2}$ , we have  $\frac{\partial \theta}{\partial t} < 0$ , while for  $\frac{\pi}{2} < \theta < \pi$ ,  $\frac{\partial \theta}{\partial t} > 0$ . Therefore, much like the case  $\mu_1 = \mu_2 = 0$  studied in [1], the fibers tend to orient themselves with the direction of extension, regardless of the value of  $\mu_2$ , given uniform initial conditions for  $h$  and  $\theta$ . Additionally, we note that  $\theta = \pm \frac{\pi}{2}$  are unstable fixed points of Eq. (4.8), while  $\theta = 0, \pi$  are stable fixed points.

We now consider the case  $\mu_1 \neq 0$ , for an initially constant  $h_i$  and  $\theta_i$ . We again have that  $\frac{\partial u}{\partial x'} = 1$  and  $h, \theta$  remain uniform for all time. However, Eq. (3.10) now yields

$$\frac{d\theta}{dt} = \frac{\sin 2\theta [2\mu_1 \sin^2 \theta - (4 + 4\mu_3 + 2\mu_2 \sin^2 \theta) \frac{1}{L}]}{4 + 4\mu_3 + \mu_2 \sin^2 2\theta}, \quad (4.9)$$

and so the evolution of the fiber direction is less clear. By again considering the cases  $0 < \theta < \frac{\pi}{2}$ ,  $\frac{\pi}{2} < \theta < \pi$ ,  $-\frac{\pi}{2} < \theta < 0$ ,  $-\pi < \theta < -\frac{\pi}{2}$  we find that in order for the fibers to align along the  $x$  axis with time, we require

$$\sin^2 \theta (L\mu_1 - \mu_2) < 2 + 2\mu_3. \quad (4.10)$$

If this condition is satisfied, fibers with angles between  $-\frac{\pi}{2} < \theta < \frac{\pi}{2}$  will rotate towards the positive  $x$  axis, with fibers outside of this range rotating towards the negative  $x$  axis, similarly to the above. However, since this expression includes  $L(t)$ , it is possible for fibers that initially rotate towards the longitudinal orientation to reverse their evolution as  $L\mu_1$  grows with time to violate (4.10). We illustrate this behavior in Fig. 6. For the choices of  $\theta_i = \frac{\pi}{4}$ ,  $L_i = h_i = 1$ ,  $\mu_1 = 5$ ,  $\mu_2 = 0$ ,  $\mu_3 = 1$ , we give the evolution of the fiber angle and evolution of the left-hand side (4.10).

## 2. Nonuniform initial fiber angles

Consider now the extension of the sheet with  $\theta(x', y', 0) = \cos(4\pi x' y') - 0.1$ ,  $h(x', 0) = 1$  and  $L(t) = 1 + t$ . We see in Fig. 7 that as the sheet is stretched, the fibers evolve towards alignment in the direction of the sheet when  $\mu_1 = 0$ . We also note that the rate at which the fibers align in this direction is enhanced in the regions of the sheet that undergo fastest thinning of the fluid.

## C. Special cases for sheets possessing active behavior

Here we briefly examine two special cases for the sheet for which  $\mu_1 > 0$ . We start by prescribing  $L(t) = 1 + t$ ,  $h_i = 1$ ,  $\mu_1 = 5$ ,  $\mu_2 = \mu_3 = 0$ , and we test two choices for the initial fiber

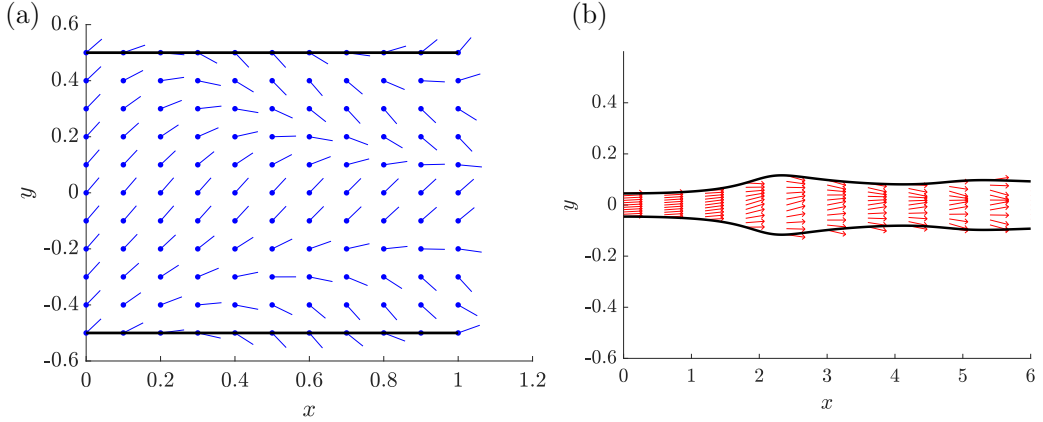


FIG. 7. (a) Initial thickness of the sheet and orientation of the fibers and (b) the thickness of the sheet and orientation of the fibers at  $t = 5$ , for the initial conditions  $h(x', 0) = 1$ ,  $\theta(x', y', 0) = \cos(4\pi x' y') - 0.1$  and choices of  $\mu_1 = \mu_3 = 0$ ,  $\mu_2 = 5$ .

angle,  $\theta_i = 0$ , corresponding to the fibers being aligned in the direction of extension, and  $\theta_i = \frac{\pi}{2}$ , corresponding to the fibers being aligned in the transverse direction in the sheet. In Fig. 8 we plot the tension required to be applied to the sheet to achieve the prescribed rate of pulling for these two choices. First, we note that there is no evolution in  $\theta$  with time. Next, we notice that for fibers arranged in the transverse direction of the sheet, the tension applied to the sheet is negative. To explain this we begin with the equation for  $u$  in spatial variables,

$$T = \int_{H^-}^{H^+} \frac{\mu_1 \cos 2\theta + (4 + 4\mu_3 + \mu_2) \frac{\partial u}{\partial x}}{4 + 4\mu_3 + \mu_2 \sin^2 2\theta} dy. \quad (4.11)$$

Now, since  $\theta$  has no evolution for these particular choices of  $\theta_i$  as they are fixed points of Eq. (3.8), then for  $\theta_i = \frac{\pi}{2}$ ,

$$T = \frac{1}{4(1 + \mu_3)} \left[ (4 + 4\mu_3 + \mu_2) \frac{\partial u}{\partial x} - \mu_1 \right] h. \quad (4.12)$$

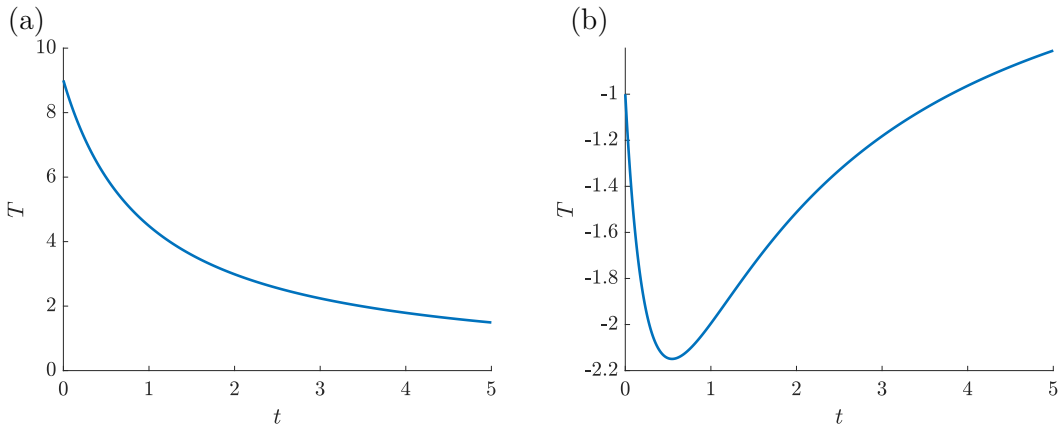


FIG. 8. Evolution of the tension applied to the sheet for two initial choices of fiber direction, (a)  $\theta_i = 0$  and (b)  $\theta_i = \frac{\pi}{2}$  up to  $t = 5$  with  $h(x', 0) = 1$ ,  $\mu_1 = 5$ ,  $\mu_2 = \mu_3 = 0$ , and prescribed pulling  $L = 1 + t$ .

It is possible that  $\mu_1 > (4 + 4\mu_3 + \mu_2)u_x$  and hence  $T < 0$ . We interpret this as being due to the fibers in the transverse direction attempting to contract the sheet, which due to mass conservation would generate a compression in the longitudinal direction, as the sheet attempts to extend longitudinally. If we define the total tension required to move the sheet at the prescribed speed as  $T_L$ , the tension caused by the fibers as  $T_f$  and the tension applied to the sheet as  $T$ , then we expect that

$$T_L = T + T_f. \quad (4.13)$$

If the rate of extension is too slow to compensate for the compression generated by the fibers pulling in the transverse direction, then  $T < 0$ . As discussed by Howell for the Newtonian case [19], when the sheet is in compression we expect buckling to occur, and the curvature of the center line will in time become significant. Thus, in this case, the nearly straight center line scaling assumed in the Green and Friedman model may be violated, and the model will no longer be valid.

#### D. Behavior of the center line

##### 1. Conditions for a flat center line

In the Newtonian problem, it was shown by Howell [19] that the center line of the sheet straightens on a timescale shorter than  $\frac{L_0}{U}$  [18,19] (and is therefore generally taken to simply be  $H = 0$ ). This is not necessarily true for a transversely isotropic fluid. It is noted in [1] that should  $\theta = \theta(x', t)$  and  $\mu_1 = \mu_2 = 0$ , then Eqs. (3.11) and (3.12) together with the requirement that  $H(0, t) = H(L(t), t) = 0$  imply that the center line must be flat. We will now demonstrate that this is also true when  $\mu_1, \mu_2 \neq 0$ . Supposing  $\theta = \theta(x', t)$ , the integrand of Eqs. (3.11) and (3.12) can be evaluated explicitly, yielding

$$\frac{\partial}{\partial x'}(hf) = 0, \quad (4.14)$$

$$\frac{\partial^2}{\partial x'^2} \left( \frac{1}{2} h^2 f \right) = \left( \frac{\partial^2 H}{\partial x'^2} + \frac{1}{2} \frac{\partial^2 h}{\partial x'^2} \right) hf, \quad (4.15)$$

where

$$f(x', t) = \frac{\mu_1 \cos 2\theta + \frac{1}{L}(4 + 4\mu_3 + \mu_2) \frac{\partial u}{\partial x'}}{4 + 4\mu_3 + \mu_2 \sin^2 2\theta}. \quad (4.16)$$

Expanding the second derivative on the left-hand side of Eq. (4.15) and using (4.14) yields that

$$\frac{\partial^2 H}{\partial x'^2} = 0, \quad (4.17)$$

and therefore  $H$  must be a straight line. It is then possible to choose our coordinate system such that  $H(x', t) \equiv 0$ .

Now let us consider what happens when  $\theta(x', y', 0) = \theta_i(y')$ , and  $\mu_1 = 0$ . In this case the equation of the center line can be written as

$$\left( \frac{\partial^2 H}{\partial x'^2} + \frac{1}{2} \frac{\partial^2 h}{\partial x'^2} \right) h G_2 \left( \frac{1}{2}, t \right) = \frac{\partial^2}{\partial x'^2} \left( h^2 \int_{-\frac{1}{2}}^{\frac{1}{2}} G_2(y', t) dy' \right). \quad (4.18)$$

We recall that, from Sec. IV A, if we choose  $\theta_i = \theta_i(y')$  only and the initial thickness  $h_i$  to be uniform, then  $G_2$  will not possess  $x'$  dependence and  $h$  will also remain uniform for all time. As a result we once again obtain (4.17), so that asymmetry in the fiber angles over the center line is not sufficient to cause an initially uniform sheet with  $\mu_1 = 0$  to deflect. We will now consider the conditions under which the center line of the sheet will not be straight.

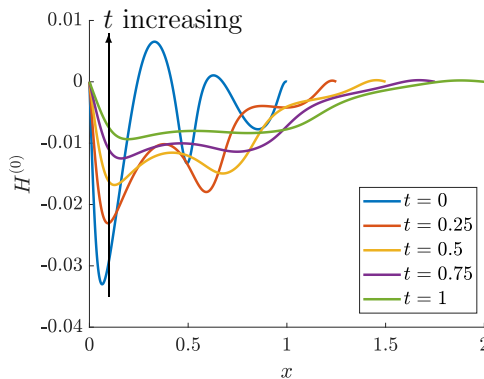


FIG. 9. Evolution of the center line of the sheet under the initial conditions  $h(x', 0) = 1$ ,  $\theta(x', y', 0) = \sin(4\pi x' y') - 0.1$  with  $\mu_2 = 5$ ,  $\mu_1 = \mu_3 = 0$ . Plotted at  $t = 0, 0.25, 0.5, 0.75, 1$ .

## 2. Conditions for a nonzero center line

For sheets possessing  $\mu_1 = 0$  and a uniform condition for the thickness of the sheet,  $h_i$ , the choice of  $\theta(x', y', 0) = \theta_i(x', y')$  being a prescribed function that is nonsymmetric (i.e.,  $\frac{\partial \theta}{\partial y'}|_{y'=0} \neq 0$ ) is required to obtain center line deflection. In Fig. 9 we give a plot of the center line evolution for the initial conditions  $\theta(x', y', 0) = \sin(4\pi x' y') - 0.1$  with  $\mu_2 = 5$ ,  $\mu_1 = \mu_3 = 0$ . We see that the center line initially possesses deflection and tends to 0. This behavior is driven by the right-hand side of (4.18) becoming small. Once this occurs, the behavior of the center line is then dominated by the  $\frac{\partial^2 h}{\partial x'^2}$  term, which itself possesses an implicit dependence on  $G_2$  through  $u$ . Additionally, for a transversely isotropic fluid with  $\mu_1 = 0$ , the deflection is small and decays quickly. Since the center line does not instantaneously collapse to 0, this suggests that considering the behavior of the fluid on a short timescale may yield some interesting behavior that is markedly different from a Newtonian fluid.

If we consider a condition for  $h(x', 0)$  that is not uniform, we find that there will exist a small deflection when  $\theta(x', y', 0) = \theta_i(y')$  only, since endowing  $h$  with  $x'$  dependence will impart  $x'$  dependence on  $\frac{\partial u}{\partial x}$  through Eq. (3.11), and hence  $\theta$  will gain  $x'$  dependence after the first time step through Eq. (3.10).

## V. RESULTS ON THE SHORT TIMESCALE

We now examine the behaviors of the sheet over a short timescale of  $t \sim \varepsilon^2 \frac{L_0}{U}$ . For a Newtonian fluid, it was demonstrated by Howell [19] that the leading order equations for the extensional flow of a slender, viscous, Newtonian sheet predict that the center line of the sheet is straight. Hence, the model cannot satisfy an initial condition in which the center line is not straight. In order to study the behavior of initially curved sheets, a short-timescale analysis is performed. The required timescale must be  $\varepsilon^2 \frac{L_0}{U}$  [18]. In the transversely isotropic problem it is similarly impossible to satisfy an arbitrary initial condition for the center line and, as we have demonstrated, there exist choices of the key parameters and initial distribution of fiber angles that give rise to a center line that is nonzero on the flow timescale. This indicates that there may exist interesting behaviors, different from the Newtonian case, over a short timescale.

### A. Short-time evolution of the center line

First, we check that the long-time behavior of the short time model is consistent with the Green and Friedman model. In Fig. 10 we give the evolution of the center line over the short timescale for the initial conditions of  $\mu_1 = \mu_3 = 0$ ,  $\mu_2 = 5$ ,  $L(0) = 1$ ,  $\theta(x, y, 0) = \sin(4\pi xy) - 0.1$ ,

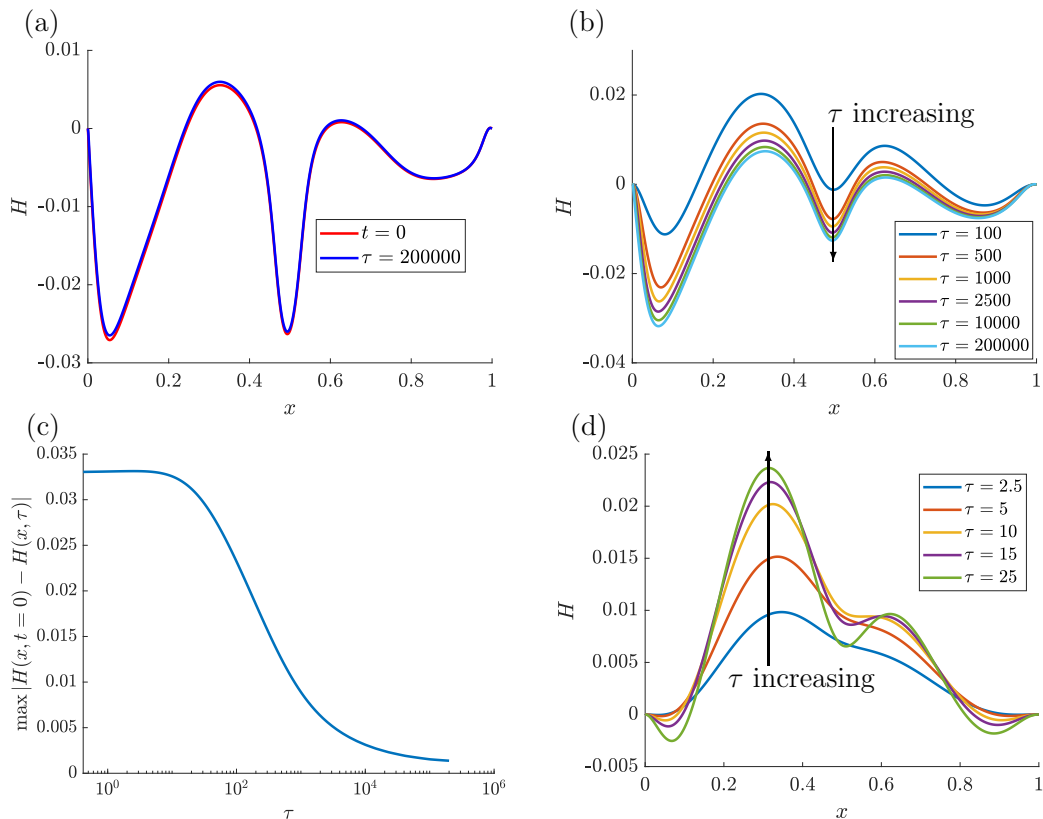


FIG. 10. Position of the center line (a) at  $t = 0$ , the initial time in the Green and Friedman model (red) and  $\tau = 200\,000$  (blue) and (b) at  $\tau = 100, 500, 1000, 2500, 10\,000, 200\,000$ , where  $\tau = 0$  is omitted as  $H(x, 0) = 0$ . In (c) we plot the maximum of the absolute difference between the evolving center line on the short timescale and the Green and Friedman result, and in (d) we give the center line at  $\tau = 2.5, 5, 10, 15, 25$ . The conditions for all of the above are  $H(x, 0) = 0$ ,  $h(x, 0) = 1$ ,  $\theta(x, y, 0) = \sin(4\pi xy) - 0.1$ ,  $\mu_1 = \mu_3 = 0$ ,  $\mu_2 = 5$ ,  $L(0) = 1$ .

$H^{(0)}(0, \tau) = H^{(0)}(L, \tau) = \frac{\partial H^{(0)}}{\partial x}(L, \tau) = \frac{\partial H^{(0)}}{\partial x}H(L, \tau) = 0$ , up to  $\tau = 200\,000$ , and compare the values of  $H(x, \tau = 200\,000)$  with  $H(x, t = 0)$ . We see that the short-timescale result closely matches the result produced by the solver for the Green and Friedman model. In Fig. 10(b) we give the evolution of the center line over  $\tau$ . Notice in Fig. 10(b) that the center line converges to the Green and Friedman model fairly quickly, and there is a small absolute difference between the center line at  $\tau = 10\,000$  and  $\tau = 200\,000$ .

For a Newtonian fluid, Howell was able to obtain an analytical expression for the decay of the center line of an initially curved sheet undergoing stretching by use of eigenfunction expansions [19], assuming the same boundary conditions we use in this section,  $H(0, \tau) = H(1, \tau) = \frac{\partial H}{\partial x}(0, \tau) = \frac{\partial H}{\partial x}(1, \tau) = 0$ . It is found that the center line decays exponentially to  $H = 0$ . The behavior for a transversely isotropic fluid is more complex. The results plotted in Fig. 10 began with the initial condition  $H(x, \tau = 0) = 0$ , and we immediately see from Fig. 10(c) that the convergence to the Green and Friedman center line is not exponential for all time. Indeed, there is an initial lag, as the center line evolves away from the flat initial condition to adopt a similar shape of the center line predicted by the Green and Friedman model, before decaying to the expected result. As an illustrative example, we include Fig. 10(d). This figure shows the formation of the peaks and troughs of the general shape of the center line given by the Green and Friedman model.

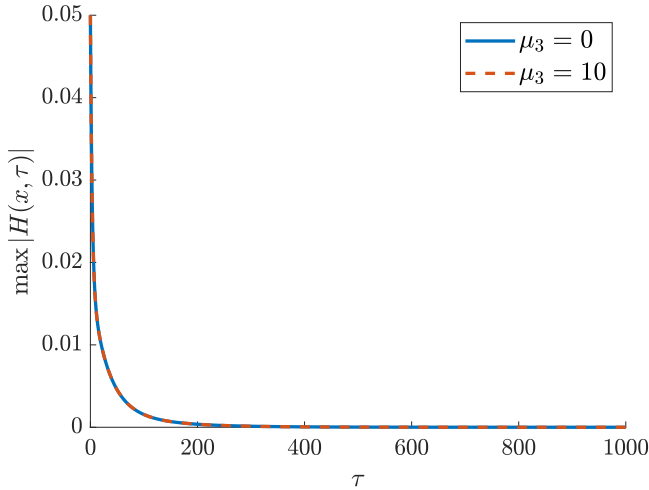


FIG. 11. Decay of the maximum value of  $H(x, \tau)$  for  $\mu_3 = 0$  (blue), and  $\mu_3 = 10$  (red) with the conditions  $H(x, 0) = \frac{1}{20}e^{-\frac{(x-0.5)^2}{0.01}}$ ,  $\mu_1 = \mu_2 = 0$ ,  $h(x, 0) = 1$ ,  $L = 1$ .

### B. Effect of key parameters upon convergence

In this subsection we discuss the effect of increasing  $\mu_2, \mu_3$  upon the convergence of the short timescale center line to the result from the Green and Friedman model. First, we note that if  $\mu_2 = 0$ ,  $\mu_3$  has no effect upon convergence. In Fig. 11 we give a plot of the decay of the maximum value of  $H(x, \tau)$  for the initial conditions of  $H(x, 0) = \frac{1}{20}e^{-\frac{(x-0.5)^2}{0.01}}$ ,  $\theta(x, y, 0) = \sin(4\pi xy)$ ,  $h(x, 0) = 1$ ,  $L = 1$ . There is no difference in the decay of the center line to flat between the Newtonian case and  $\mu_3 = 10$ .

Now choosing  $\mu_2 > 0$ , in Fig. 12 we plot the maximum absolute difference across the sheet between the center line on the short timescale and the result obtained by solving Eq. (3.12) for varied values of  $\mu_2, \mu_3$  with the conditions  $h(x, 0) = 1$ ,  $\theta(x, y, 0) = \sin(4\pi xy) - 0.1$ ,  $\mu_1 = 0$ ,  $\mu_2 = 5$ ,  $L(0) = 1$ . First, in Fig. 12(a) we fix  $\mu_3 = 0$  and vary  $\mu_2$  (note the case of  $\mu_2 = 5$  corresponds to the example given above). We see that as  $\mu_2$  increases, the difference between the

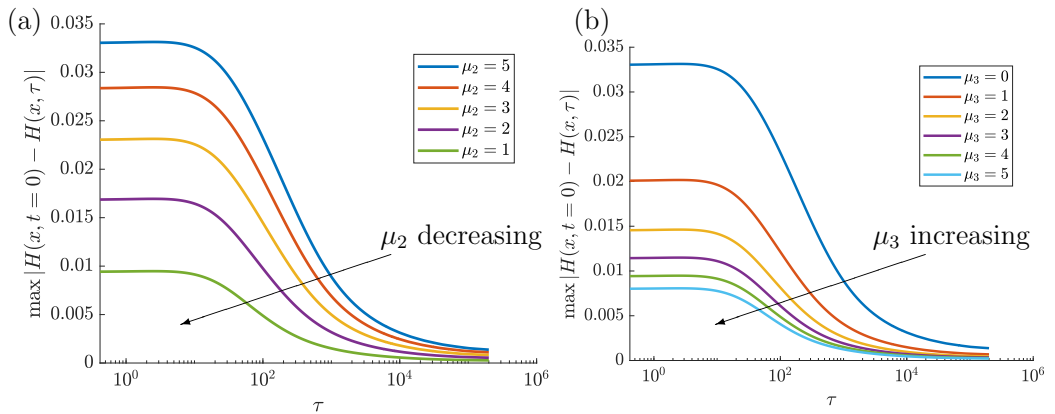


FIG. 12. Maximum absolute difference across the sheet between the center line on the short timescale and the result obtained by solving Eq. (3.12) for (a)  $\mu_3 = 0$ ,  $\mu_2 = 1, 2, 3, 4, 5$  and (b)  $\mu_2 = 5$ ,  $\mu_3 = 1, 2, 3, 4, 5$ , with the conditions  $H(x, 0) = 0$ ,  $h(x, 0) = 1$ ,  $\theta(x, y, 0) = \sin(4\pi xy) - 0.1$ ,  $\mu_1 = 0$ ,  $L(0) = 1$ .

flat initial condition of the center line and the result of the Green and Friedman model also increases. This is due to the deepening of the trough around  $x = 0.5$  seen in Fig. 10(a). We note that changing  $\mu_2$  does not appear to affect the length of the lag as the center line is adopting the correct general shape before decaying, but as  $\mu_2$  increases, the decay is faster. In Fig. 12(b) we fix  $\mu_2 = 5$  and vary  $\mu_3$  (as before, the case of  $\mu_3 = 0$  corresponds to the example given above). Once again, we see that the effect of increasing  $\mu_3$  has little affect upon the timing of the convergence of the center line, and that the behavior we see here is a consequence of the role of  $\mu_3$  in moderating the effects of  $\mu_2$  in the Green and Friedman model as discussed in Sec. IV.

## VI. DISCUSSION

In this paper we have constructed and employed a numerical strategy to solve the model proposed by Green and Friedman for the extensional flow of a thin 2D sheet of a fiber-reinforced fluid, first reducing the model by eliminating  $u^{(1)}$  and then employing an arbitrary Lagrangian-Eulerian method. We have shown how the distribution of fibers within the fluid can cause interesting non-Newtonian behaviors such as driving nonuniformity in the development of the thickness of an initially uniform sheet and deflection of the center line even with the implicit assumption that the center line is nearly straight. Our results also show that the bulk properties of a passive transversely isotropic fluid sheet are controlled largely by the behavior of a derived “effective viscosity.”

As far as the behavior of an active transversely isotropic fluid is concerned, preliminarily we have seen that allowing  $\mu_1 \neq 0$  allows the fibers to develop towards alignments that are not in the direction of extension of the fluid. However, if the fibers are aligned in the longitudinal direction of the sheet and possesses active behavior, the tension within the sheet is increased. Active behavior giving rise to greater tension has been observed in the seeding of hydrogels with a suspension of self-aligning cells [32]. Future work in this area could include constructing a more biologically realistic multiphase model that incorporates the work in this paper as a fibrous extracellular matrix or hydrogel, with the cells exhibiting active behavior instead of the fibers. This could result in a model of how different experimental setups lead to different alignment patterns of cells and could determine the best conditions to grow neural tissue.

There are a number of other avenues for further work related to this paper. We model sheets that are nearly straight, with the employment of a Cartesian coordinate system restricting the model to examining sheets which are initially slightly curved, i.e.,  $\frac{H}{L_0}$  is small. Where this is not the case, future work could entail the use of a curvilinear coordinate system to approach sheets with curvature in the center line in work similar to Ribe [21]. As the sheet starts to become very thin, there may be a new regime where the  $\mu_1$  term in (3.11) dominates the  $\frac{\partial u}{\partial x'}$  term. Perhaps the behavior of the sheet in this regime may shed light upon how the active behavior of the fluid may drive breakup of the sheet. Simpler modifications could include prescribing the tension applied to the ends of the sheet, rather than prescribing the length. Furthermore we could also modify the model to include the effects of surface tension, inertia, and body forces.

## ACKNOWLEDGMENT

M.H. thanks the University of Birmingham School of Mathematics for funding given in his Ph.D. Studentship and the University of Adelaide for funding given in his Beacon of Enlightenment Scholarship.

The authors declare that they have no competing interests.

## APPENDIX A: MODEL EQUATIONS IN FULL

To briefly summarize, the dimensionless equations are

$$\frac{\partial u}{\partial x} + \frac{\partial v}{\partial y} = 0, \tag{A1}$$



for conservation of mass, with the momentum equation (2.2) yielding in the  $x$  direction:

$$\begin{aligned}
 & -\varepsilon^2 \frac{\partial p}{\partial x} + \frac{\partial^2 u}{\partial y^2} + \varepsilon^2 \frac{\partial^2 u}{\partial x^2} + \varepsilon^2 \mu_1 \frac{\partial}{\partial x} (\cos^2 \theta) + \varepsilon \mu_1 \frac{\partial}{\partial y} (\cos \theta \sin \theta) \\
 & + \mu_2 \frac{\partial}{\partial x} \left[ \varepsilon^2 \cos^4 \theta \frac{\partial u}{\partial x} + \cos^3 \theta \sin \theta \left( \varepsilon \frac{\partial u}{\partial y} + \varepsilon^3 \frac{\partial v}{\partial x} \right) + \varepsilon^2 \cos^2 \theta \sin^2 \theta \frac{\partial v}{\partial y} \right] \\
 & + 2\mu_3 \frac{\partial}{\partial x} \left[ 2\varepsilon^2 \cos^2 \theta \frac{\partial u}{\partial x} + \cos \theta \sin \theta \left( \varepsilon \frac{\partial u}{\partial y} + \varepsilon^3 \frac{\partial v}{\partial x} \right) \right] \\
 & + \mu_2 \frac{\partial}{\partial y} \left\{ \cos \theta \sin \theta \left[ \varepsilon \cos^2 \theta \frac{\partial u}{\partial x} + \cos \theta \sin \theta \left( \frac{\partial u}{\partial y} + \varepsilon^2 \frac{\partial v}{\partial x} \right) + \varepsilon \sin^2 \theta \frac{\partial v}{\partial y} \right] \right\} \\
 & + \mu_3 \frac{\partial}{\partial y} \left( \frac{\partial u}{\partial y} + \varepsilon^2 \frac{\partial v}{\partial x} \right) = 0,
 \end{aligned}$$

while in the  $y$  direction we have

$$\begin{aligned}
 & -\varepsilon \frac{\partial p}{\partial y} + \varepsilon^3 \frac{\partial^2 v}{\partial x^2} + \varepsilon \frac{\partial^2 v}{\partial y^2} + \varepsilon \mu_1 \frac{\partial}{\partial y} (\sin^2 \theta) + \varepsilon^2 \mu_1 \frac{\partial}{\partial x} (\cos \theta \sin \theta) \\
 & + \mu_2 \frac{\partial}{\partial y} \left[ \varepsilon \sin^2 \theta \cos^2 \theta \frac{\partial u}{\partial x} + \cos \theta \sin^3 \theta \left( \frac{\partial u}{\partial y} + \varepsilon^2 \frac{\partial v}{\partial x} \right) + \varepsilon \sin^4 \theta \frac{\partial v}{\partial y} \right] \\
 & + 2\mu_3 \frac{\partial}{\partial y} \left[ 2\varepsilon \sin^2 \theta \frac{\partial v}{\partial y} + \cos \theta \sin \theta \left( \frac{\partial u}{\partial y} + \varepsilon^2 \frac{\partial v}{\partial x} \right) \right] \\
 & + \mu_2 \frac{\partial}{\partial x} \left[ \varepsilon^2 \sin \theta \cos^3 \theta \frac{\partial u}{\partial x} + \cos^2 \theta \sin^2 \theta \left( \varepsilon \frac{\partial u}{\partial y} + \varepsilon^3 \frac{\partial v}{\partial x} \right) + \varepsilon^2 \cos \theta \sin^3 \theta \frac{\partial v}{\partial y} \right] \\
 & + \mu_3 \frac{\partial}{\partial x} \left( \varepsilon \frac{\partial u}{\partial y} + \varepsilon^3 \frac{\partial v}{\partial x} \right) = 0, \tag{A2}
 \end{aligned}$$

with the fiber director field being given by

$$\varepsilon \frac{\partial \theta}{\partial t} + \varepsilon u \frac{\partial \theta}{\partial x} + \varepsilon v \frac{\partial \theta}{\partial y} = -\varepsilon \sin \theta \cos \theta \frac{\partial u}{\partial x} - \sin^2 \theta \frac{\partial u}{\partial y} + \varepsilon^2 \cos^2 \theta \frac{\partial v}{\partial x} + \varepsilon \sin \theta \cos \theta \frac{\partial v}{\partial y}. \tag{A3}$$

## APPENDIX B: SIMPLIFICATION OF THE EQUATION FOR $\theta$

In the main text, we claimed that Eq. (3.8) permitted great simplification by noting that the equation corresponded only to advection in a purely horizontal direction of the reference domain. To demonstrate this simplification, suppose  $\tilde{\theta}(x', y', t)$  is a function defined over  $D_{\text{ref}}$  that satisfies the advection equation

$$\frac{\partial \tilde{\theta}}{\partial t} + \tilde{u} \frac{\partial \tilde{\theta}}{\partial x'} = \tilde{f}, \tag{B1}$$

where  $\tilde{u}(x', t)$  and  $\tilde{f}(x', t)$  are a horizontal advection velocity and forcing term, respectively. We can relate  $\theta(x, y, t) = \tilde{\theta}(x(x', t), y(x', y', t), t)$ , and using the mapping  $\Phi$ , which gives

$$\frac{\partial \tilde{\theta}}{\partial t} = \frac{\partial \theta}{\partial t} + \frac{\dot{L}x}{L} \frac{\partial \theta}{\partial x} + \left\{ \frac{\partial H}{\partial t} + \left( \frac{y-H}{h} \right) \frac{\partial h}{\partial t} + \frac{\dot{L}x}{L} \left[ \frac{\partial H}{\partial x} + \left( \frac{y-H}{h} \right) \frac{\partial h}{\partial x} \right] \right\} \frac{\partial \theta}{\partial y}, \tag{B2}$$

$$\frac{\partial \tilde{\theta}}{\partial x'} = L \frac{\partial \theta}{\partial x} + L \left[ \frac{\partial H}{\partial x} + \left( \frac{y-H}{h} \right) \frac{\partial h}{\partial x} \right] \frac{\partial \theta}{\partial y}. \tag{B3}$$

Substituting (B2) and (B3) into (B1) then yields

$$\frac{\partial \theta}{\partial t} + \frac{\partial \theta}{\partial x} \left( L\tilde{u} + \frac{\dot{L}x}{L} \right) + \frac{\partial \theta}{\partial y} \left\{ \frac{\partial H}{\partial t} + \left( \frac{y-H}{h} \right) \frac{\partial h}{\partial t} + \left[ \frac{\partial H}{\partial x} + \left( \frac{y-H}{h} \right) \frac{\partial h}{\partial x} \right] \left( L\tilde{u} + \frac{\dot{L}x}{L} \right) \right\} = \tilde{f}, \quad (\text{B4})$$

and we now choose  $u(x, t) = L\tilde{u} + \frac{\dot{L}x}{L}$ , in order to recover the correct coefficient of  $\frac{\partial \theta}{\partial x}$ . Examining the coefficient of the  $\frac{\partial \theta}{\partial y}$  term we note that

$$\frac{\partial H}{\partial t} + \left( \frac{y-H}{h} \right) \frac{\partial h}{\partial t} + u \left[ \frac{\partial H}{\partial x} + \left( \frac{y-H}{h} \right) \frac{\partial h}{\partial x} \right] \quad (\text{B5})$$

$$= \frac{\partial H}{\partial t} + u \frac{\partial H}{\partial x} + \left( \frac{y-H}{h} \right) \left( -h \frac{\partial u}{\partial x} \right) \quad (\text{B6})$$

$$= \frac{\partial H}{\partial t} + \frac{\partial}{\partial x} (uH) - y \frac{\partial u}{\partial x} = v, \quad (\text{B7})$$

where we have used the equation for conservation of mass, (2.7), to obtain (B6). Here we have demonstrated that the coefficient of  $\theta_y$  is precisely  $v$  when mapping back from  $D_{ref}$  to the original domain. Therefore, we have shown that the advection of  $\theta$  is purely horizontal upon the reference domain, with velocity  $\tilde{u}(x', t) = \frac{u-Lx'}{L} = \frac{u-u_{mesh}}{L}$ .

### APPENDIX C: DISCRETIZATION OF THE GREEN AND FRIEDMAN INTEGRAL EQUATIONS

In what follows, the treatment of the integral equations is in the Eulerian framework. The integral equations (3.11) and (3.12) require further treatment before being discretized and solved. We discretize with

$$\theta^{(0)}(x_i, y_j, \tau_k) = \theta_{i,j}^k, \text{ etc.}, \quad (\text{C1})$$

where  $i = 1 : M + 1$ ,  $j = 1 : N + 1$ ,  $k = 1 : T + 1$  where  $M, N$  are the number of steps in the  $x, y$  directions and  $T$  is the number of time steps. The Green and Friedman model was typically solved with  $\Delta x = \frac{1}{M}$ ,  $\Delta y = \frac{1}{N}$ ,  $\Delta t = \frac{1}{2T}$ ,  $M = N = 800$ ,  $T = 1600$ , with the Courant-Friedrichs-Lewy condition checked at each time step. Now, introduce

$$F(x, y, t) = \frac{\mu_1 \cos 2\theta + (4 + 4\mu_3 + \mu_2)u_x}{4 + 4\mu_3 + \mu_2 \sin^2 2\theta}, \quad (\text{C2})$$

and it will be convenient to write  $F = F_1 + u_x F_2$ , where

$$F_1 = \frac{\mu_1 \cos 2\theta}{4 + 4\mu_3 + \mu_2 \sin^2 2\theta}, \quad F_2 = \frac{4 + 4\mu_3 + \mu_2}{4 + 4\mu_3 + \mu_2 \sin^2 2\theta}; \quad (\text{C3})$$

in much the same way, we also introduce notation for the integrals of  $F$  by defining  $G = G_1 + u_x G_2$ , where

$$G_m(x, y, t) = \int_{H^-}^y F_m(x, s, t) ds, \quad (\text{C4})$$

for  $m = 1, 2$ . Equation (3.11) can now be written as

$$0 = \frac{\partial}{\partial x} [G_1(x, H^+, t) + u_x(x, t)G_2(x, H^+, t)], \quad (\text{C5})$$

using the trapezoidal rule,

$$G_m(x, H^+, t) = \frac{h(x, t)}{N-1} \left( \frac{F_m(x, y_0, t) + F_m(x, y_{N-1}, t)}{2} + \sum_{i=1}^{N-2} F_m(x, y_i, t) \right), \quad (\text{C6})$$

where  $N$  is the number of nodes in the  $y$  direction. We note that upon substituting the trapezoidal rule into (C5), the result does not depend on  $H$ . That is, its presence in the integration limits is redundant and effectively just describes a vertical translation. Therefore,  $H$  is decoupled from the rest of the system, and we can solve the equations for  $u$  and  $\theta$  and then compute  $H$  as required at a desired time. For completeness, we include the discretization for Eq. (C5). First, introduce the notation

$$[G_m]_{i,N-1}^k = G_m(x_i, H_i^k + h_i^k/2, t_k); \quad (\text{C7})$$

now (C5) gives, through centered finite differences,

$$\begin{aligned} & \frac{[G_1]_{i-1,N-1}^k - [G_1]_{i+1,N-1}^k}{2L/(M-1)} \\ &= \frac{[G_2]_{i+1,N-1}^k - [G_2]_{i-1,N-1}^k}{2L/(M-1)} \frac{u_{i+1}^k - u_i^k}{2L/(M-1)} + \frac{u_i^k - 2u_i^k + u_{i-1}^k}{(L/(M-1))^2} [G_2]_{i,N-1}^k, \end{aligned} \quad (\text{C8})$$

where  $N, M$  are the number of nodes in the vertical and horizontal directions, respectively, so that  $i = 0 : M-1, j = 0 : N-1$ . Noting that  $u_0^k = 0, u_{M-1}^k = \dot{L}(t_k)$ , and that  $G_m$  is readily precomputed at each time step  $k$ , yields a tridiagonal system for  $u^k$ . If we now consider the equation for  $H$  (3.9), this is the only equation in the model that is indeed easier to treat in the Eulerian framework than the ALE. Using Eq. (2.12) and the Leibniz rule we may write Eq. (2.9) as

$$0 = -\left(H_{xx} + \frac{h_{xx}}{2}\right)G(x, H^+, t) + \frac{\partial^2}{\partial x^2} \int_{H^-}^{H^+} G(x, y, t) dy; \quad (\text{C9})$$

in order to proceed, one must apply the trapezoidal rule twice to each  $G_m$ . Applying it once yields

$$\int_{H^-}^{H^+} G_m(x, y, t) dy = \frac{h(x, t)}{N-1} \left( \frac{G_m(x, y_0, t) + G_m(x, y_{N-1}, t)}{2} + \sum_{j=1}^{N-2} G_m(x, y_j, t) \right), \quad (\text{C10})$$

then, for each  $j > 0$ ,

$$G_m(x, y_j, t) = \frac{h(x, t)}{N-1} \left( \frac{F_m(x, y_0, t) + F_m(x, y_j, t)}{2} + \sum_{i=1}^{j-1} F_m(x, y_i, t) \right), \quad (\text{C11})$$

for the case  $j = 0, G_m(x, y_0, t) = 0$ . Substitution of (C11) into (C10) yields

$$\begin{aligned} \int_{H^-}^{H^+} G_m(x, y, t) dy &= \left(\frac{h}{N-1}\right)^2 \left( \frac{2N-3}{4} F_m(x, y_0, t) + \frac{1}{4} F_m(x, y_{N-1}, t) \right. \\ &\quad \left. + \sum_{j=1}^{N-2} (N-1-j) F_m(x, y_j, t) \right). \end{aligned} \quad (\text{C12})$$

Finally, we require the introduction of the notation

$$[IG_m]_i^k = \int_{H^-}^{H^+} G_m(x_i, y, t_k) dy, \quad (\text{C13})$$

for  $m = 1, 2$ . Clearly, we use (C12) to precompute  $[IG_m]$  at the required nodes as necessary. The discretization of Eq. (C9) is then

$$\begin{aligned}
 & \frac{H_{i-1}^k - 2H_i^k + H_{i+1}^k}{[L(t_k)/(M-1)]^2} \left( [G_1]_i^k + \frac{u_{i+1}^k - u_{i-1}^k}{2L(t_k)/(M-1)} [G_2]_i^k \right) \\
 &= -\frac{h_{i-1}^k - 2h_i^k + h_{i+1}^k}{2[L(t_k)/(M-1)]^2} \left( [G_1]_i^k + \frac{u_{i+1}^k - u_{i-1}^k}{2L(t_k)/(M-1)} [G_2]_i^k \right) + \frac{[IG_1]_{i-1}^k - 2[IG_1]_i^k + [IG_1]_{i+1}^k}{[L(t_k)/(M-1)]^2} \\
 &+ \frac{u_{i+2}^k - 2u_{i+1}^k + 2u_{i-1}^k - u_{i-2}^k}{2[L(t_k)/(M-1)]^3} [IG_2]_{i+1}^k + \frac{u_{i+1}^k - 2u_i^k + u_{i-1}^k}{[L(t_k)/(M-1)]^2} \frac{[IG_2]_{i+1}^k - [IG_2]_{i-1}^k}{2L(t_k)/(M-1)} \\
 &+ \frac{[IG_2]_{i+1}^k - 2[IG_2]_i^k + [IG_2]_{i-1}^k}{[L(t_k)/(M-1)]^2} \frac{u_{i+1}^k - u_{i-1}^k}{2L(t_k)/(M-1)}. \tag{C14}
 \end{aligned}$$

Equation (C14) contains wholly precomputable quantities on the right-hand side. Therefore, similar to the equation for  $u$ , this creates a tridiagonal system to be solved for  $H$ . For the specific cases of  $i = 0, M-1$ , we have the boundary condition that  $H_0^k = H_{M-1}^k = 0$ . For the cases of  $i = 1, M-2$ , the discretization must be modified slightly as the stencil for  $u_{xxx}$  is too wide. This can be done in a number of ways and is omitted.

#### APPENDIX D: DERIVATION OF THE SHORT-TIMESCALE INTEGRAL EQUATIONS

In order to close the model, we must go to yet higher orders in order to obtain equations for  $u^{(0)}, H^{(0)}$ . Our approach is to integrate the relevant equations over the depth of the sheet and apply the no-stress boundary conditions at  $y = H^{(0)\pm}$ . We find that a number of higher order terms in the boundary conditions will be eliminated by substitution of previously obtained quantities. The  $\mathcal{O}(\varepsilon^3)$   $x$ -momentum equation is

$$\begin{aligned}
 & \frac{\partial}{\partial x} \left\{ -p^{(0)} + 2\frac{\partial u^{(0)}}{\partial x} + \mu_1 \cos^2 \theta^{(0)} \right. \\
 & \quad \left. + \mu_2 \left[ \cos^4 \theta^{(0)} \frac{\partial u^{(0)}}{\partial x} + \cos^3 \theta^{(0)} \sin \theta^{(0)} \left( \frac{\partial u^{(1)}}{\partial y} + \frac{\partial V^{(1)}}{\partial x} \right) + \cos^2 \theta^{(0)} \sin^2 \theta^{(0)} \frac{\partial V^{(2)}}{\partial y} \right] \right. \\
 & \quad \left. + 2\mu_3 \left[ 2\cos^2 \theta^{(0)} \frac{\partial u^{(0)}}{\partial x} + \cos \theta^{(0)} \sin \theta^{(0)} \left( \frac{\partial u^{(1)}}{\partial y} + \frac{\partial V^{(1)}}{\partial x} \right) \right] \right\} - \frac{\partial^2 u^{(0)}}{\partial x^2} \\
 &= -\frac{\partial}{\partial y} \left\{ \frac{\partial u^{(2)}}{\partial y} + \frac{\partial V^{(2)}}{\partial x} + \mu_1 (\theta^{(1)} \cos 2\theta^{(0)}) + \mu_2 \left[ \cos^3 \theta^{(0)} \sin \theta^{(0)} \frac{\partial u^{(1)}}{\partial x} \right. \right. \\
 & \quad \left. \left. + \theta^{(1)} (\cos^4 \theta^{(0)} - 3\sin^2 \theta^{(0)} \cos^2 \theta^{(0)}) \frac{\partial u^{(0)}}{\partial x} + \cos^2 \theta^{(0)} \sin^2 \theta^{(0)} \left( \frac{\partial u^{(2)}}{\partial y} + \frac{\partial V^{(2)}}{\partial x} \right) \right. \right. \\
 & \quad \left. \left. + \frac{1}{2} \theta^{(1)} \sin 4\theta^{(0)} \left( \frac{\partial u^{(1)}}{\partial y} + \frac{\partial V^{(1)}}{\partial x} \right) + \cos \theta^{(0)} \sin^3 \theta^{(0)} \frac{\partial V^{(3)}}{\partial y} \right. \right. \\
 & \quad \left. \left. + \theta^{(1)} (3\sin^2 \theta^{(0)} \cos^2 \theta^{(0)} - \sin^4 \theta^{(0)}) \frac{\partial V^{(2)}}{\partial y} \right] + \mu_3 \left( \frac{\partial u^{(2)}}{\partial y} + \frac{\partial V^{(2)}}{\partial x} \right) \right\} + \frac{\partial^2 V^{(2)}}{\partial x \partial y}, \tag{D1}
 \end{aligned}$$

and its associated no-stress boundary condition is

$$\begin{aligned}
 & \frac{\partial u^{(2)}}{\partial y} + \frac{\partial V^{(2)}}{\partial x} + \mu_1 \theta^{(1)} \cos 2\theta^{(0)} \\
 & + \mu_2 \left[ \cos^3 \theta^{(0)} \sin \theta^{(0)} \frac{\partial u^{(1)}}{\partial x} + \theta^{(1)} (\cos^4 \theta^{(0)} - 3 \sin^2 \theta^{(0)} \cos^2 \theta^{(0)}) \frac{\partial u^{(0)}}{\partial x} \right. \\
 & + \cos^2 \theta^{(0)} \sin^2 \theta^{(0)} \left( \frac{\partial u^{(2)}}{\partial y} + \frac{\partial V^{(2)}}{\partial x} \right) + \frac{1}{2} \theta^{(1)} \sin 4\theta^{(0)} \left( \frac{\partial u^{(1)}}{\partial y} + \frac{\partial V^{(1)}}{\partial x} \right) \\
 & \left. + \cos \theta^{(0)} \sin^3 \theta^{(0)} \frac{\partial V^{(3)}}{\partial y} + \theta^{(1)} (3 \sin^2 \theta^{(0)} \cos^2 \theta^{(0)} - \sin^4 \theta^{(0)}) \frac{\partial V^{(2)}}{\partial y} \right] + \mu_3 \left( \frac{\partial V^{(2)}}{\partial x} + \frac{\partial u^{(2)}}{\partial y} \right) \\
 & = \left( \frac{\partial H^{(0)}}{\partial x} \pm \frac{1}{2} \frac{\partial h^{(0)}}{\partial x} \right) \left\{ -p^{(0)} + 2 \frac{\partial u^{(0)}}{\partial x} + \mu_1 \cos^2 \theta^{(0)} \right. \\
 & + \mu_2 \left[ \cos^4 \theta^{(0)} \frac{\partial u^{(0)}}{\partial x} + \cos^3 \theta^{(0)} \sin \theta^{(0)} \left( \frac{\partial u^{(1)}}{\partial y} + \frac{\partial V^{(1)}}{\partial x} \right) + \cos^2 \theta^{(0)} \sin^2 \theta^{(0)} \frac{\partial V^{(2)}}{\partial y} \right] \\
 & \left. \times 2\mu_3 \left[ 2 \cos^2 \theta^{(0)} \frac{\partial u^{(0)}}{\partial x} + \cos \theta^{(0)} \sin \theta^{(0)} \left( \frac{\partial u^{(1)}}{\partial y} + \frac{\partial V^{(1)}}{\partial x} \right) \right] \right\} \quad \text{on } y = H^{(0)\pm}. \quad (\text{D2})
 \end{aligned}$$

We note that the remaining terms outside of the derivatives in (D1) cancel due to the continuity equation at  $\mathcal{O}(\varepsilon^2)$ . Integrating Eq. (D1) over the depth of the sheet yields

$$\int_{H^{(0)-}}^{H^{(0)+}} \frac{\partial}{\partial x} [-p^{(0)} + g_1(x, \tau)] dy = - \left[ \frac{\partial u^{(2)}}{\partial y} + \frac{\partial V^{(2)}}{\partial x} + g_2(x, \tau) \right]_{y=H^{(0)-}}^{y=H^{(0)+}}, \quad (\text{D3})$$

where  $g_1, g_2$  are functions containing the collected  $\mu_1, \mu_2, \mu_3$  terms from (D1) and are readily obtained by inspection. Application of (D2) now yields

$$\begin{aligned}
 & \int_{H^{(0)-}}^{H^{(0)+}} \frac{\partial}{\partial x} (-p^{(0)} + g_1) dy \\
 & = \left( \frac{\partial H^{(0)}}{\partial x} - \frac{1}{2} \frac{\partial h^{(0)}}{\partial x} \right) (-p^{(0)} + g_1)_{y=H^{(0)-}} - \left( \frac{\partial H^{(0)}}{\partial x} + \frac{1}{2} \frac{\partial h^{(0)}}{\partial x} \right) (-p^{(0)} + g_1)_{y=H^{(0)+}}, \quad (\text{D4})
 \end{aligned}$$

and hence by use of the Leibniz rule, we now obtain an equation for  $\bar{u}$ ,

$$\begin{aligned}
 & \frac{\partial}{\partial x} \int_{H^{(0)-}}^{H^{(0)+}} \left\{ 4 \frac{\partial u^{(0)}}{\partial x} + \mu_1 \cos 2\theta^{(0)} + \mu_2 \left[ \cos^2 2\theta^{(0)} \frac{\partial u^{(0)}}{\partial x} \right. \right. \\
 & \left. \left. + \frac{1}{4} \sin 4\theta^{(0)} \left( \frac{\partial u^{(1)}}{\partial y} + \frac{\partial V^{(1)}}{\partial x} \right) \right] + 4\mu_3 \frac{\partial u^{(0)}}{\partial x} \right\} dy = 0. \quad (\text{D5})
 \end{aligned}$$

A similar process at  $\mathcal{O}(\varepsilon^4)$  yields an equation for  $H$ ,

$$\begin{aligned}
 & \frac{\partial}{\partial x} \int_{H^{(0)-}}^{H^{(0)+}} \frac{\partial}{\partial x} \int_{H^{(0)-}}^y \left[ 4 \frac{\partial u^{(0)}}{\partial x} + \mu_1 \cos 2\theta^{(0)} + \mu_2 \cos^2 2\theta^{(0)} \frac{\partial u^{(0)}}{\partial x} \right. \\
 & \left. + \frac{\mu_2}{4} \sin 4\theta^{(0)} \left( \frac{\partial u^{(1)}}{\partial y} + \frac{\partial V^{(1)}}{\partial x} \right) + 4\mu_3 \frac{\partial u^{(0)}}{\partial x} \right] dy' dy = 0. \quad (\text{D6})
 \end{aligned}$$

We note that these equations are of the same form as Eqs. (2.8) and (2.9), with the difference being that  $u^{(0)}$  now possesses  $y$  dependence. Substitution of (2.12) and (2.27) into both (D5) and (D6) and use of the Leibniz rule upon (D6) yield Eqs. (2.28) and (2.29).

## APPENDIX E: DISCRETIZATION OF THE SHORT TIMESCALE MODEL

In this Appendix we give the discretization of the integral equations in the system of the short timescale equations, namely, (3.19) and (3.20). As before, we drop the superscript notation for leading-order quantities. We discretize using the same notation as detailed in Appendix C. As before, the short timescale was typically solved with  $\Delta x = \frac{1}{M}$ ,  $\Delta y = \frac{1}{N}$ ,  $M = N = 800$ , with the Courant-Friedrichs-Lewy condition checked at each time step. The length of the time step was varied. The range of size of time steps was  $\Delta \tau = \frac{1}{1600}$  for  $\tau < 100$  up to  $\Delta \tau = 100$  for  $\tau = 200\,000$ . Similarly to the discretization of the Green and Friedman model equations, we define

$$Z_1(x, y, \tau) = \int_{-\frac{1}{2}}^y \frac{\mu_1 \cos 2\theta}{4 + 4\mu_3 + \mu_2 \sin^2 2\theta} h d\tilde{y}, \quad (\text{E1})$$

$$Z_2(x, y, \tau) = \int_{-\frac{1}{2}}^y \frac{4 + 4\mu_3 + \mu_2}{4 + 4\mu_3 + \mu_2 \sin^2 2\theta} h d\tilde{y}, \quad (\text{E2})$$

$$J(x, t) = \int_{-\frac{1}{2}}^{\frac{1}{2}} \frac{(4 + 4\mu_3 + \mu_2)h^2 y'}{4 + 4\mu_3 + \mu_2 \sin^2 2\theta} d\tilde{y}, \quad (\text{E3})$$

and we note that the definitions of  $Z_1, Z_2$  here are similar to  $G_1, G_2$  in Appendix C but are not precisely the same. It is possible to obtain  $G_1, G_2$  from  $Z_1, Z_2$  by undoing both the transformation  $y = H + h\tilde{y}$  and the short timescale. Since the ALE transformation in Sec. III acts as a linear transformation on the integral equations, one may treat  $Z_1, Z_2$  as the integrals in ALE form on the short timescale. We may now rewrite Eq. (3.19) as

$$\begin{aligned} Z_2\left(x, \frac{1}{2}, \tau\right) \frac{\partial^2 \bar{u}}{\partial x^2} + \frac{\partial Z_2(x, \frac{1}{2}, \tau)}{\partial x} \frac{\partial \bar{u}}{\partial x} + \frac{\partial^2 H}{\partial x \partial \tau} \left( \frac{\partial Z_2(x, \frac{1}{2}, \tau)}{\partial x} \frac{\partial H}{\partial x} + Z_2\left(x, \frac{1}{2}, \tau\right) \frac{\partial^2 H}{\partial x^2} \right) \\ + \frac{\partial^3 H}{\partial x^2 \partial \tau} \left( Z_2\left(x, \frac{1}{2}, \tau\right) \frac{\partial H}{\partial x} - \frac{\partial J}{\partial x} \right) - J \frac{\partial^4 H}{\partial x^3 \partial \tau} = - \frac{\partial Z_1(x, \frac{1}{2}, \tau)}{\partial x}. \end{aligned} \quad (\text{E4})$$

We choose to use a FTCS finite difference method, hence the discretization of (E4) is

$$\begin{aligned} [Z_2]_{i,N-1}^k \frac{\bar{u}_{i+1}^k - 2\bar{u}_i^k + \bar{u}_{i-1}^k}{\Delta x^2} + \frac{[Z_2]_{i+1,N-1}^k - [Z_2]_{i-1,N-1}^k}{2\Delta x} \frac{\bar{u}_{i+1}^k - \bar{u}_{i-1}^k}{2\Delta x} \\ + \frac{(H_{i+1}^{k+1} - H_{i-1}^{k+1}) - (H_{i+1}^k - H_{i-1}^k)}{2\Delta \tau \Delta x} \left( \frac{[Z_2]_{i+1,N-1}^k - [Z_2]_{i-1,N-1}^k}{2\Delta x} \frac{H_{i+1}^k - H_{i-1}^k}{2\Delta x} \right. \\ \left. + [Z_2]_{i,N-1}^k \frac{H_{i+1}^k - 2H_i^k + H_{i-1}^k}{\Delta x^2} \right) \\ + \frac{(H_{i+1}^{k+1} - 2H_i^{k+1} + H_{i-1}^{k+1}) - (H_{i+1}^k - 2H_i^k + H_{i-1}^k)}{\Delta \tau \Delta x^2} \left( [Z_2]_{i,N-1}^k \frac{H_{i+1}^k - H_{i-1}^k}{2\Delta x} \right. \\ \left. - \frac{J_{i+1}^k - J_{i-1}^k}{2\Delta x} \right) - J_i^k \frac{(H_{i+2}^{k+1} - 2H_{i+1}^{k+1} + 2H_{i-1}^{k+1} - H_{i-2}^{k+1}) - (H_{i+2}^k - 2H_{i+1}^k + 2H_{i-1}^k - H_{i-2}^k)}{2\Delta \tau \Delta x^3} \\ = - \frac{[Z_1]_{i+1,N-1}^k - [Z_1]_{i-1,N-1}^k}{2\Delta x}. \end{aligned} \quad (\text{E5})$$

This discretization can be written in the matrix form

$$\Delta \tau \Delta x^2 \mathbf{b} + \mathbf{M}_H \mathbf{H}^k = \mathbf{M}_H \mathbf{H}^{k+1} + \Delta \tau \Delta x \mathbf{M}_U \bar{\mathbf{u}}^k, \quad (\text{E6})$$

where  $\mathbf{H}^k = (H_1^k, H_2^k, \dots, H_{N+1}^k)^T$ ,  $\bar{\mathbf{u}}^k = (\bar{u}_1^k, \bar{u}_2^k, \dots, \bar{u}_{N+1}^k)^T$ , and  $\mathbf{M}_H, \mathbf{M}_{\bar{u}}$  are matrices whose entries are the coefficients of the  $H^{k+1}$  and  $\bar{u}^k$  terms, respectively, and are dependent upon the choice of discretization of the  $x$  derivatives of  $H, \bar{u}$ . We note that the left-hand side of (E6) is known and precomputable at each time step. Due to the  $\frac{\partial H^k}{\partial x^3 \partial \tau}$  term, the stencil must be adjusted at the ends of the domain by using biased finite differences.

Next, we define more functions for notational convenience:

$$IZ_1(x, \tau) = \int_{-\frac{1}{2}}^{\frac{1}{2}} \int_{-\frac{1}{2}}^{\bar{y}} \frac{\mu_1 \cos 2\theta}{4 + 4\mu_3 + \mu_2 \sin^2 2\theta} h^2 d\bar{y}' d\bar{y}, \quad (\text{E7})$$

$$IZ_2(x, \tau) = \int_{-\frac{1}{2}}^{\frac{1}{2}} \int_{-\frac{1}{2}}^{\bar{y}} \frac{4 + 4\mu_3 + \mu_2}{4 + 4\mu_3 + \mu_2 \sin^2 2\theta} h^2 d\bar{y}' d\bar{y}, \quad (\text{E8})$$

$$K(x, \tau) = \int_{-\frac{1}{2}}^{\frac{1}{2}} \int_{-\frac{1}{2}}^{\bar{y}} \frac{(4 + 4\mu_3 + \mu_2) h^3 \bar{y}'}{4 + 4\mu_3 + \mu_2 \sin^2 2\theta} d\bar{y}' d\bar{y}. \quad (\text{E9})$$

With the introduced functions, we may express (3.20) as

$$\begin{aligned} & IZ_2 \frac{\partial^3 \bar{u}}{\partial x^3} + 2 \frac{\partial IZ_2}{\partial x} \frac{\partial^2 \bar{u}}{\partial x^2} + \frac{\partial \bar{u}}{\partial x} \left[ \frac{\partial^2 IZ_2}{\partial x^2} - Z_2 \left( \frac{\partial^2 H}{\partial x^2} + \frac{1}{2} \frac{\partial^2 h}{\partial x^2} \right) \right] - K \frac{\partial^5 H}{\partial x^4 \partial \tau} + \frac{\partial^4 H}{\partial x^3 \partial \tau} \left( IZ_2 \frac{\partial H}{\partial x} - 2 \frac{\partial K}{\partial x} \right) \\ & + \frac{\partial^3 H}{\partial x^2 \partial \tau} \left[ 2IZ_2 \frac{\partial^2 H}{\partial x^2} + 2 \frac{\partial IZ_2}{\partial x} \frac{\partial H}{\partial x} + J \left( \frac{\partial^2 H}{\partial x^2} + \frac{1}{2} \frac{\partial^2 h}{\partial x^2} \right) - \frac{\partial^2 K}{\partial x^2} \right] \\ & + \frac{\partial^2 H}{\partial x \partial \tau} \left[ IZ_2 \frac{\partial^3 H}{\partial x^3} + 2 \frac{\partial IZ_2}{\partial x} \frac{\partial^2 H}{\partial x^2} + \frac{\partial^2 IZ_2}{\partial x^2} \frac{\partial H}{\partial x} - Z_2 \frac{\partial H}{\partial x} \left( \frac{\partial^2 H}{\partial x^2} + \frac{1}{2} \frac{\partial^2 h}{\partial x^2} \right) \right] \\ & = Z_1 \left( \frac{\partial^2 H}{\partial x^2} + \frac{1}{2} \frac{\partial^2 h}{\partial x^2} \right) - \frac{\partial^2 IZ_1}{\partial x^2}. \end{aligned} \quad (\text{E10})$$

The discretization of (E10) is

$$\begin{aligned} & [IZ_2]_i^k \frac{\bar{u}_{i+2}^k - 2\bar{u}_{i+1}^k + 2\bar{u}_{i-1}^k - \bar{u}_{i-2}^k}{2\Delta x^3} \\ & + \frac{[IZ_2]_{i+1}^k - [IZ_2]_{i-1}^k}{\Delta x} \frac{\bar{u}_{i+1}^k - 2\bar{u}_i^k + \bar{u}_{i-1}^k}{\Delta x^2} + \frac{\bar{u}_{i+1}^k - \bar{u}_{i-1}^k}{2\Delta x} \left[ \frac{[IZ_2]_{i+1}^k - 2[IZ_2]_i^k + [IZ_2]_{i-1}^k}{\Delta x^2} \right. \\ & \left. - Z_2 \left( \frac{H_{i+1}^k - 2H_i^k + H_{i-1}^k}{\Delta x^2} + \frac{1}{2} \frac{h_{i+1}^k - 2h_i^k + h_{i-1}^k}{\Delta x^2} \right) \right] + \frac{(H_{i+1}^{k+1} - H_{i-1}^{k+1}) - (H_{i+1}^k - H_{i-1}^k)}{2\Delta \tau \Delta x} \\ & \times \left[ \frac{[IZ_2]_{i+1}^k - 2[IZ_2]_i^k + [IZ_2]_{i-1}^k}{\Delta x^2} \frac{H_{i+1}^k - H_{i-1}^k}{2\Delta x} + \frac{[IZ_2]_{i+1}^k - [IZ_2]_{i-1}^k}{\Delta x} \right. \\ & \times \frac{H_{i+1}^k - 2H_i^k + H_{i-1}^k}{\Delta x^2} + [IZ_2]_i^k \frac{H_{i+2}^k - 2H_{i+1}^k + 2H_{i-1}^k - H_{i-2}^k}{2\Delta x^3} - Z_2^k \frac{H_{i+1}^k - H_{i-1}^k}{2\Delta x} \\ & \left. \times \left( \frac{H_{i+1}^k - 2H_i^k + H_{i-1}^k}{\Delta x^2} + \frac{1}{2} \frac{h_{i+1}^k - 2h_i^k + h_{i-1}^k}{\Delta x^2} \right) \right] \\ & + \frac{(H_{i+1}^{k+1} - 2H_i^{k+1} + H_{i-1}^{k+1}) - (H_{i+1}^k - 2H_i^k + H_{i-1}^k)}{\Delta \tau \Delta x^2} \left[ 2[IZ_2]_i^k \frac{H_{i+1}^k - 2H_i^k + H_{i-1}^k}{\Delta x^2} \right. \\ & \left. + \frac{IZ_{2i+1} - IZ_{2i-1}}{\Delta x} \frac{H_{i+1}^k - H_{i-1}^k}{2\Delta x} - \frac{K_{i+1}^k - 2K_i^k + K_{i-1}^k}{\Delta x^2} \right] \end{aligned}$$

$$\begin{aligned}
 & + J_i^k \left( \frac{H_{i+1}^k - 2H_i^k + H_{i-1}^k}{\Delta x^2} + \frac{1}{2} \frac{h_{i+1}^k - 2h_i^k + h_{i-1}^k}{\Delta x^2} \right) \\
 & + \frac{(H_{i+2}^{k+1} - 2H_{i+1}^{k+1} + 2H_{i-1}^{k+1} - H_{i-2}^{k+1}) - (H_{i+2}^k - 2H_{i+1}^k + 2H_{i-1}^k - H_{i-2}^k)}{2\Delta\tau\Delta x^3} \\
 & \times \left( IZ_{2i}^k \frac{H_{i+1}^k - H_{i-1}^k}{2\Delta x} - \frac{K_{i+1}^k - K_{i-1}^k}{2\Delta x} \right) \\
 & - K_i^k \frac{(H_{i+2}^{k+1} - 4H_{i+1}^{k+1} + 6H_i^{k+1} - 4H_{i-1}^{k+1} + H_{i-2}^{k+1}) - (H_{i+2}^k - 4H_{i+1}^k + 6H_i^k - 4H_{i-1}^k + H_{i-2}^k)}{\Delta\tau\Delta x^4} \\
 = & Z_i^k \left( \frac{H_{i+1}^k - 2H_i^k + H_{i-1}^k}{\Delta x^2} + \frac{1}{2} \frac{h_{i+1}^k - 2h_i^k + h_{i-1}^k}{\Delta x^2} \right) - \frac{IZ_{2i+1}^k - 2IZ_{2i}^k + IZ_{2i-1}^k}{\Delta x^2}. \tag{E11}
 \end{aligned}$$

As before, we may write (E11) in the form

$$\Delta\tau\Delta x^2\mathbf{c} + \mathbf{M}'_{\mathbf{H}}\mathbf{H}^k = \mathbf{M}'_{\mathbf{H}}\mathbf{H}^{k+1} + \Delta\tau\Delta x\mathbf{M}'_{\mathbf{U}}\bar{\mathbf{u}}^k, \tag{E12}$$

where the coefficients of all  $H^{k+1}$ ,  $\bar{\mathbf{u}}^k$  terms are entries within  $\mathbf{M}'_{\mathbf{H}}$ ,  $\mathbf{M}'_{\mathbf{U}}$ , respectively.

In our implementation, the matrices  $\mathbf{M}'_{\mathbf{U}}$ ,  $\mathbf{M}'_{\mathbf{H}}$  are a quintuple banded matrices. The additional derivative in  $H$  does not change the size of the stencil. We include the boundary conditions for  $H$  in the first two and final two lines of both matrices, so that it is not necessary to adjust the stencil near the endpoints of the domain. Hence, we can construct the linear system

$$\begin{pmatrix} \mathbf{M}_{\mathbf{H}} & \Delta\tau\Delta x\mathbf{M}'_{\mathbf{U}} \\ \mathbf{M}'_{\mathbf{H}} & \Delta\tau\Delta x\mathbf{M}'_{\mathbf{U}} \end{pmatrix} \begin{pmatrix} \mathbf{H}^{k+1} \\ \bar{\mathbf{u}}^k \end{pmatrix} = \begin{pmatrix} \Delta\tau\Delta x^2\mathbf{b} + \mathbf{M}_{\mathbf{H}}\mathbf{H}^k \\ \Delta\tau\Delta x^2\mathbf{c} + \mathbf{M}'_{\mathbf{H}}\mathbf{H}^k \end{pmatrix}. \tag{E13}$$

This linear system is solved at each  $k$ , with Eq. (II.20) requiring  $H^{k+1}$  in order to update  $\theta^k \rightarrow \theta^{k+1}$ .

- 
- [1] J. E. F. Green and A. Friedman, The extensional flow of a thin sheet of incompressible, transversely isotropic fluid, *Eur. J. Appl. Math.* **19**, 225 (2008).
- [2] G. Cupples, R. J. Dyson, and D. J. Smith, Viscous propulsion in active transversely isotropic media, *J. Fluid Mech.* **812**, 501 (2017).
- [3] L. J. Cummings, Evolution of a thin film of nematic liquid crystal with anisotropic surface energy, *Eur. J. Appl. Math.* **15**, 651 (2004).
- [4] F. C. Chretien and G. David, Temporary obstructive effect of human cervical mucus on spermatozoa throughout reproductive life: A scanning electron microscopic study, *Eur. J. Obstet. Gynecol. Reprod. Biol.* **8**, 307 (1978).
- [5] J. L. Ericksen, Transversely isotropic fluids, *Kolloid Z.* **173**, 117 (1960).
- [6] A. J. M. Spencer, Fibre-streamline flows of fibre-reinforced viscous fluids, *Eur. J. Appl. Math.* **8**, 209 (1997).
- [7] M. E. M. Lee and H. Ockendon, A continuum model for entangled fibres, *Eur. J. Appl. Math.* **16**, 145 (2005).
- [8] R. J. Dyson, J. E. F. Green, J. P. Whiteley, and H. M. Byrne, An investigation of the influence of extracellular matrix anisotropy and cell–matrix interactions on tissue architecture, *J. Math. Biol.* **72**, 1775 (2016).
- [9] R. J. Dyson and O. E. Jensen, A fibre-reinforced fluid model of anisotropic plant cell growth, *J. Fluid Mech.* **655**, 472 (2010).



- [10] B. D. Hull, T. G. Rogers, and A. J. M. Spencer, Theory of fibre buckling and wrinkling in shear flows of fibre-reinforced composites, *Compos. Manuf.* **2**, 185 (1991).
- [11] T. G. Rogers, Squeezing flow of fibre-reinforced viscous fluids, *J. Eng. Math.* **23**, 81 (1989).
- [12] E. Evans-Hoeker, D. A. Pritchard, D. L. Long, A. H. Herring, J. B. Stanford, and A. Z. Steiner, Cervical mucus monitoring prevalence and associated fecundability in women trying to conceive, *Fertil. Steril.* **100**, 1033 (2013).
- [13] K. S. Moghissi, The function of the cervix in fertility, *Fertil. Steril.* **23**, 295 (1972).
- [14] D. P. Wolf, L. Blasco, M. A. Khan, and M. Litt, Human cervical mucus. IV. Viscoelasticity and sperm penetrability during the ovulatory menstrual cycle, *Fertil. Steril.* **30**, 163 (1978).
- [15] P. D. Howell, Models for thin viscous sheets, *Eur. J. Appl. Math.* **7**, 321 (1996).
- [16] J. Eggers and T. F. Dupont, Drop formation in a one-dimensional approximation of the Navier–Stokes equation, *J. Fluid Mech.* **262**, 205 (1994).
- [17] Y. M. Stokes, B. H. Bradshaw-Hajek, and E. O. Tuck, Extensional flow at low Reynolds number with surface tension, *J. Eng. Math.* **70**, 321 (2011).
- [18] J. D. Buckmaster, A. Nachman, and L. Ting, The buckling and stretching of a viscida, *J. Fluid Mech.* **69**, 1 (1975).
- [19] P. D. Howell, Extensional thin layer flows, Ph.D. thesis, University of Oxford, 1994.
- [20] N. M. Ribe, Bending and stretching of thin viscous sheets, *J. Fluid Mech.* **433**, 135 (2001).
- [21] N. M. Ribe, A general theory for the dynamics of thin viscous sheets, *J. Fluid Mech.* **457**, 255 (2002).
- [22] G. Pfingstag, B. Audoly, and A. Boudaoud, Thin viscous sheets with inhomogeneous viscosity, *Phys. Fluids* **23**, 063103 (2011).
- [23] J. Chakraborty, J. Luo, and R. J. Dyson, Lockhart with a twist: Modelling cellulose microfibril deposition and reorientation reveals twisting plant cell growth mechanisms, *J. Theor. Biol.* **525**, 110736 (2021).
- [24] C. R. Holloway, R. J. Dyson, and D. J. Smith, Linear Taylor–Couette stability of a transversely isotropic fluid, *Proc. R. Soc. A* **471**, 20150141 (2015).
- [25] C. R. Holloway, D. J. Smith, and R. J. Dyson, Linear Rayleigh–Bénard stability of a transversely isotropic fluid, *Eur. J. Appl. Math.* **30**(4), 659 (2019).
- [26] C. R. Holloway, G. Cupples, D. J. Smith, J. E. F. Green, R. J. Clarke, and R. J. Dyson, Influences of transversely isotropic rheology and translational diffusion on the stability of active suspensions, *R. Soc. Open Sci.* **5**, 180456 (2018).
- [27] N. Phan-Thien and A. L. Graham, A new constitutive model for fibre suspensions: Flow past a sphere, *Rheol. Acta* **30**, 44 (1991).
- [28] N. Phan-Thien and A. L. Graham, The squeezing flow of a model suspension fluid, *Rheol. Acta* **29**, 433 (1990).
- [29] A. J. M. Spencer, *Deformations of Fibre-Reinforced Materials* (Oxford University Press, New York, 1972).
- [30] J. Donea, A. Huerta, J. P. Ponthot, and A. Rodríguez-Ferran, Arbitrary Lagrangian–Eulerian methods, in *Encyclopedia of Computational Mechanics*, 2nd ed., edited by E. Stein, R. Borst, and T. J. R. Hughes (John Wiley & Sons, Hoboken, New Jersey, 2017), pp. 1–23.
- [31] J. J. Wylie, B. H. Bradshaw-Hajek, and Y. M. Stokes, The evolution of a viscous thread pulled with a prescribed speed, *J. Fluid Mech.* **795**, 380 (2016).
- [32] M. Antman-Passig, S. Levy, C. Gartenberg, H. Schori, and O. Shefi, Mechanically oriented 3D collagen hydrogel for directing neurite growth, *Tissue Eng. Part A* **23**, 403 (2017).